

Discretized Fast-Slow Systems near Transcritical Singularities

Maximilian Engel* and Christian Kuehn*

19th June 2018

Abstract

We extend slow manifolds near a transcritical singularity in a fast-slow system given by the explicit Euler discretization of the corresponding continuous-time normal form. The analysis uses the blow-up method and direct trajectory-based estimates. We prove that the qualitative behaviour is preserved by a time-discretization with sufficiently small step size. This step size is fully quantified relative to the time scale separation. Our proof also yields the continuous-time results as a special case and provides more detailed calculations in the classical (or scaling) chart.

Keywords: transcritical bifurcation, slow manifolds, invariant manifolds, loss of normal hyperbolicity, blow-up method, discretization, maps.

Mathematics Subject Classification (2010): 34E15, 34E20, 37M99, 37G10, 34C45, 39A99.

1 Introduction

We study the dynamics of the two-dimensional quadratic map

$$p : \begin{pmatrix} x \\ y \end{pmatrix} \mapsto \begin{pmatrix} \tilde{x} \\ \tilde{y} \end{pmatrix} = \begin{pmatrix} x + h(x^2 - y^2 + \lambda\varepsilon) \\ y + \varepsilon h \end{pmatrix} \quad (1.1)$$

for $h, \varepsilon > 0$. We interpret ε as a small time scale separation parameter between the fast variable x and the slow variable y . The parameter h can be viewed as the step size for the explicit Euler discretization of the corresponding ordinary differential equation (ODE)

$$\begin{aligned} x' &= x^2 - y^2 + \lambda\varepsilon, \\ y' &= \varepsilon, \end{aligned} \quad (1.2)$$

which represents the normal form of a fast-slow system exhibiting a *transcritical singularity* at the origin. The term transcritical refers to the fact that, if y is seen as a bifurcation parameter for the flow in the x -variable, a transcritical bifurcation occurs at the origin $(x, y) = (0, 0)$. The

*Zentrum Mathematik der TU München, Boltzmannstr. 3, D-85748 Garching bei München

origin is singular since hyperbolicity of the dynamics breaks down at this point. The same holds for the map (1.1).

In the case of (1.2), Krupa and Szmolyan [15] analyze the dynamics around the origin by using the *blow-up method* for vector fields with singularities. The key idea to use the blow-up method [3, 4] for fast-slow systems goes back to Dumortier and Roussarie [5]. They observed that this technique may convert non-hyperbolic singularities at which fast and slow directions interact into partially hyperbolic problems. The method inserts a suitable manifold, e.g. a sphere, at the singularity and describes the extension of hyperbolic objects through a neighbourhood of the singularity via the partially hyperbolic dynamics on this manifold; see e.g. [18, Chapter 7] for an introduction and [21, 20, 22, 9, 14, 17, 19] for a list of a few, yet by no means exhaustive, list of different applications to planar fast-slow systems.

Krupa and Szmolyan also used the blow-up method for normal form of *fold singularities* in fast-slow systems [14]. For this case Nipp and Stoffer [25] transform the blow-up technique to the corresponding explicit Runge-Kutta, in particular Euler, discretization and prove the extension of slow manifolds for the discrete time system around the singularity. They treat the discretized dynamics in vicinity to the fold singularity as an application of a more general existence theory for invariant manifolds they develop in [25].

In this paper, we use instead a direct approach to analyze, how trajectories induced by (1.1) pass the singularity at the origin. This approach allows us to obtain pathwise control over the transitions in and within the different blow-up charts. The singularity is blown up to a sphere on which trajectories can be described directly via the map. This leads to the main result of the paper, Theorem 3.1, which is the discrete-time extension of [15, Theorem 2.1]. In this context, we only impose that h is bounded by ε and prove that there is no further restriction on the step size. Our theorem states explicitly, how for the cases $\lambda < 1$ and $\lambda > 1$ in (1.1) attracting slow manifolds extend beyond the singularity at the origin. It gives estimates on the contraction rates of neighbourhoods of the manifolds. The case $\lambda = 1$ corresponds with the problem of *canard solutions* [1, 5, 16] and will be dealt with in future work. It should be noted that, by letting $h \rightarrow 0$, our proof of Theorem 3.1 can also be seen as a different way of proving [15, Theorem 2.1] and our proof makes the results [15] for the scaling chart more explicit. Additionally, the blow-up method provides the insight that only in one chart around the singularity the preservation of stability behaviour is bound to the stability criteria of the Euler discretisation derived from the Dahlquist test equation while in the other charts there is no such restriction.

This work lays the foundation of a broader effort to apply the blow-up method, which has so far mainly been used for flows, to fast-slow dynamical systems induced by maps. First, it is insightful to look at key examples that can be compared to continuous-time analogues, as in the case of the transcritical singularity. In the future, also multiscale discrete-time problems, which have no correspondence to fast-slow flows, will be considered.

The remainder of the paper is structured as follows. In Section 2, we summarize the results of Krupa and Szmolyan for transcritical singularities in continuous time [15]. We state and explain their main result Theorem 2.1 in Section 2.1, and we outline the main ingredients of the proof in Section 2.2 thereby introducing the basic ideas of the blow-up technique. In Section 3, we discuss the problem in discrete time associated with (1.1). Our main result is Theorem 3.1. The ingredients of the proof are developed in the following subsections. Section 3.1 introduces the blow-up method for the new discrete setting and, subsequently, the dynamics are analyzed in three different charts of the manifold that blows up the singularity, leading to the proof of Theorem 3.1. In Section 3.2, we describe how trajectories enter a neighbourhood of the origin

via the *entrance chart* K_1 and leave this neighbourhood in the case of $\lambda < 1$. Section 3.3 builds the core of the proof: we analyze, how trajectories pass the origin depending on λ in the *scaling chart* K_2 . In Section 3.4, the *exit* dynamics through chart K_3 are described for the case $\lambda > 1$. Finally, in Section 3.5 we combine the findings of the previous sections to finish the proof of Theorem 3.1. We conclude with a short summary of our results and an outlook on future work in Section 4.

Acknowledgements: CK and ME gratefully acknowledge support by the DFG via the SFB/TR109 Discretization in Geometry and Dynamics.

2 Transcritical singularity in continuous time

We start with a brief review and notation for continuous-time fast-slow systems. Consider a system of singularly perturbed ordinary differential equations (ODEs) of the form

$$\begin{aligned} \varepsilon \frac{dx}{d\tau} &= \varepsilon \dot{x} = f(x, y, \varepsilon), \\ \frac{dy}{d\tau} &= \dot{y} = g(x, y, \varepsilon), \quad x \in \mathbb{R}^m, \quad y \in \mathbb{R}^n, \quad 0 < \varepsilon \ll 1, \end{aligned} \quad (2.1)$$

where f, g , are C^k -functions with $k \geq 3$. Since ε is a small parameter, the variables x and y are often called the *fast* variable(s) and the *slow* variable(s) respectively. The time variable in (2.1), denoted by τ , is termed the *slow* time scale. The change of variables to the *fast* time scale $t := \tau/\varepsilon$ transforms the system (2.1) into the ODEs

$$\begin{aligned} x' &= f(x, y, \varepsilon), \\ y' &= \varepsilon g(x, y, \varepsilon). \end{aligned} \quad (2.2)$$

Both equations correspond with a respective limiting problem for $\varepsilon = 0$: the *reduced problem* (or *slow subsystem*) is given by

$$\begin{aligned} 0 &= f(x, y, 0), \\ \dot{y} &= g(x, y, 0), \end{aligned} \quad (2.3)$$

and the *layer problem* (or *fast subsystem*) is

$$\begin{aligned} x' &= f(x, y, 0), \\ y' &= 0. \end{aligned} \quad (2.4)$$

We can understand the reduced problem (2.3) as a dynamical system on the *critical manifold*

$$S_0 = \{(x, y) \in \mathbb{R}^{n+m} : f(x, y, 0) = 0\}.$$

Observe that the manifold S_0 consists of equilibria of the layer problem (2.4). S_0 is called *normally hyperbolic* if the matrix $D_x f(p) \in \mathbb{R}^{m \times m}$ for all $p \in S_0$ has no spectrum on the imaginary axis. For a normally hyperbolic S_0 *Fenichel Theory* [7, 13, 18, 27] implies that for ε sufficiently small, there is a locally invariant slow manifold S_ε such that the restriction of (2.1) to S_ε is a regular perturbation of the reduced problem (2.3). Furthermore, it follows from Fenichel's perturbation results that S_ε possesses an invariant stable and unstable foliation, where the dynamics behave as a small perturbation of the layer problem (2.4).

A challenging phenomenon is the breakdown of normal hyperbolicity of S_0 such that Fenichel Theory cannot be applied. Typical examples of such a breakdown are found at bifurcation points $p \in S_0$, where the Jacobian $D_x f(p)$ has at least one eigenvalue with zero real part. The simplest examples are folds or points of transversal self-intersection of S in planar systems ($m = 1 = n$). In the following we focus on the *transcritical* bifurcation in planar systems.

2.1 Dynamics near the transcritical singularity

We briefly recall the main results for transcritical fast-slow singularities in the continuous-time setting from [15]. Without loss of generality, i.e., up to translation of coordinates, we may just assume that the transcritical point coincides with the origin. Consider the system of planar ODEs on the fast time scale

$$\begin{aligned} x' &= f(x, y, \varepsilon), \\ y' &= \varepsilon g(x, y, \varepsilon), \end{aligned} \tag{2.5}$$

where the vector field f satisfies the following conditions at the origin:

$$f(0, 0, 0) = 0, \quad \frac{\partial}{\partial x} f(0, 0, 0) = 0, \quad \frac{\partial}{\partial y} f(0, 0, 0) = 0$$

These conditions imply that the critical manifold $S := S_0 = \{(x, y) \in \mathbb{R}^2 : f(x, y, 0) = 0\}$ has a self-intersection at the origin. The condition

$$\det H_f((0, 0, 0)) < 0,$$

where H_f denotes the Hessian matrix of f in x, y , implies that this intersection is non-degenerate. Moreover, we require

$$\frac{\partial^2 f}{\partial^2 x}(0, 0, 0) \neq 0$$

to guarantee that S is transverse to the critical fibre $\{(x, 0) : x \in \mathbb{R}\}$. Furthermore, we assume that

$$g(0, 0, 0) \neq 0$$

to ensure transversal slow dynamics at the origin. The transcritical bifurcation at the origin, induced by such a system, can be brought [15] to the normal form

$$\begin{aligned} x' &= x^2 - y^2 + \lambda\varepsilon + \mathcal{R}_1(x, y, \varepsilon), \\ y' &= \varepsilon(1 + \mathcal{R}_2(x, y, \varepsilon)), \end{aligned} \tag{2.6}$$

where $\lambda > 0$ is a constant and

$$\mathcal{R}_1(x, y, \varepsilon) = \mathcal{O}(x^3, x^2y, xy^2, y^3, \varepsilon x, \varepsilon y, \varepsilon^2), \quad \mathcal{R}_2(x, y, \varepsilon) = \mathcal{O}(x, y, \varepsilon).$$

The critical manifold S is the union of four branches. We denote them by $S_a^+, S_a^-, S_r^+, S_r^-$ where a means attracting and r repelling with respect to the fast variables and $+$ and $-$ correspond to the sign of the y -variable, see also Figure 1. We denote the corresponding slow manifolds for small $\varepsilon > 0$ by $S_{a,\varepsilon}^+, S_{a,\varepsilon}^-, S_{r,\varepsilon}^+, S_{r,\varepsilon}^-$. We focus on the fate of $S_{a,\varepsilon}^-$, when it is continued through a neighbourhood of $(0, 0)$. For that purpose, we fix $\rho > 0$ and let J be a small open interval around 0 in \mathbb{R} , potentially depending on ε . Then one can define

$$\Delta^{\text{in}} := \{(-\rho, y), y + \rho \in J\}, \quad \Delta_a^{\text{out}} = \{(-\rho, y), y - \rho \in J\}, \quad \Delta_e^{\text{out}} = \{(\rho, y), y \in J\}.$$

If Π_a and Π_e denote the transition maps from Δ^{in} to Δ_a^{out} and Δ_e^{out} respectively, we can formulate the main result on the transcritical singularity [15, Theorem 2.1].

Theorem 2.1. *Fix $\lambda \neq 1$. There exists $\varepsilon_0 > 0$ such that the following assertions hold for $\varepsilon \in [0, \varepsilon_0)$.*

(T1) If $\lambda > 1$, then the manifold $S_{a,\varepsilon}^-$ passes through Δ_e^{out} at a point $(\rho, h(\varepsilon))$ where $h(\varepsilon) = \mathcal{O}(\sqrt{\varepsilon})$. The section Δ^{in} is mapped by Π_e to an interval containing $S_{a,\varepsilon}^- \cap \Delta_e^{\text{out}}$ of size $\mathcal{O}(e^{-C/\varepsilon})$, where C is a positive constant.

(T2) If $\lambda < 1$, then the section Δ^{in} (including the point $\Delta^{\text{in}} \cap S_{a,\varepsilon}^-$) is mapped by Π_a to an interval about $S_{a,\varepsilon}^+$ of size $\mathcal{O}(e^{-C/\varepsilon})$, where C is a positive constant.

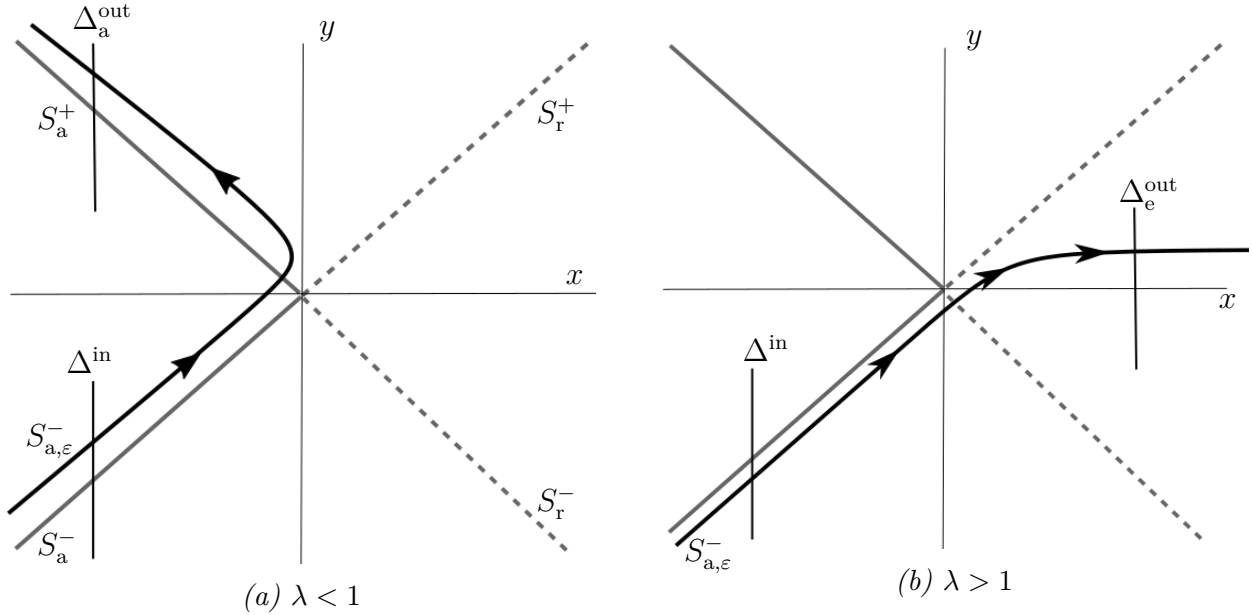


Figure 1: Extension of the slow manifold $S_{a,\varepsilon}^-$ (black curve) for the system (2.6) around the non-hyperbolic singularity at the origin for $\lambda < 1$ and $\lambda > 1$. The four parts of the critical manifold are indicated as well (grey lines), where attracting parts are solid lines and repelling ones dashed lines. The two sketches illustrate the different cases in Theorem 2.1.

In the following, we are going to sketch the proof of Theorem 2.1 to illustrate the setting for the continuous-time case [15] and to be able to have this case available for comparison. To start, we consider ε as variable, and write the problem in three variables

$$\begin{aligned} x' &= x^2 - y^2 + \lambda\varepsilon + \mathcal{R}_1(x, y, \varepsilon), \\ y' &= \varepsilon(1 + \mathcal{R}_2(x, y, \varepsilon)), \\ \varepsilon' &= 0. \end{aligned} \tag{2.7}$$

The total derivative of the above vector field X in (x, y, ε) has only zero eigenvalues at the origin $(x, y, \varepsilon) = (0, 0, 0)$. In particular, the origin is a non-hyperbolic equilibrium. To gain hyperbolicity at the singularity one can use the *blow-up method*, which maps the equilibrium point to an entire manifold, on which the dynamics can be desingularized. The shortest proof of Theorem 2.1 uses the quasi-homogeneous *blow-up transformation*

$$x = r\bar{x}, \quad y = r\bar{y}, \quad \varepsilon = r^2\bar{\varepsilon},$$

where $(\bar{x}, \bar{y}, \bar{\varepsilon}, r) \in B := S^2 \times [0, r_0]$ for some $r_0 > 0$. The transformation can be formalized as a map $\Phi : B \rightarrow \mathbb{R}^3$, where r_0 is small enough such that the dynamics on $\Phi(B)$ can be described by the normal form approximation. The map Φ induces a vector field \bar{X} on B by $\Phi_*(\bar{X}) = X$,

where Φ_* is the pushforward induced by Φ . Note that, since $\Phi(B)$ is a full neighbourhood of the origin, it suffices to study the vector field \bar{X} . The associated dynamics on B are best analysed in three charts K_i , $i = 1, 2, 3$, an entrance ($\bar{x} = -1$), a scaling ($\bar{\varepsilon} = 1$) and an exit ($\bar{x} = 1$) chart, given by

$$K_1 : \quad x = -r_1, \quad y = r_1 y_1, \quad \varepsilon = r_1^2 \varepsilon_1, \quad (2.8)$$

$$K_2 : \quad x = r_2 x_2, \quad y = r_2 y_2, \quad \varepsilon = r_2^2, \quad (2.9)$$

$$K_3 : \quad x = r_3, \quad y = r_3 y_3, \quad \varepsilon = r_3^2 \varepsilon_3. \quad (2.10)$$

The changes of coordinates between the charts look as follows: $k_{12} : K_1 \rightarrow K_2$ is given by

$$x_2 = -\varepsilon_1^{-1/2}, \quad y_2 = \varepsilon_1^{-1/2} y_1, \quad r_2 = \varepsilon_1^{1/2} r_1, \quad (2.11)$$

$k_{21} : K_2 \rightarrow K_1$ is given by

$$\varepsilon_1 = x_2^{-2}, \quad y_1 = -x_2^{-1} y_2, \quad r_1 = -x_2 r_2, \quad (2.12)$$

$k_{32} : K_3 \rightarrow K_2$ is given by

$$x_2 = \varepsilon_3^{-1/2}, \quad y_2 = \varepsilon_3^{-1/2} y_3, \quad r_2 = \varepsilon_3^{1/2} r_3, \quad (2.13)$$

and $k_{23} : K_2 \rightarrow K_3$ is given by

$$\varepsilon_3 = x_2^{-2}, \quad y_3 = x_2^{-1} y_2, \quad r_3 = x_2 r_2. \quad (2.14)$$

2.2 Describing the dynamics via the blow-up method

The dynamics in K_1 and K_3 can be desingularised. Indeed, the origin is mapped to a sphere $S^2 \times \{r = 0\}$, and dividing the three vector fields by r_i for $i = 1, 3$ and using a time change yield:

$$\begin{aligned} r_1' &= -r_1 F_1(r_1, y_1, \varepsilon_1), \\ y_1' &= \varepsilon_1 + y_1 F_1(r_1, y_1, \varepsilon_1) + \mathcal{O}(r_1), \\ \varepsilon_1' &= 2\varepsilon_1 F_1(r_1, y_1, \varepsilon_1), \end{aligned} \quad (2.15)$$

where $F_1(y_1, \varepsilon_1) = 1 - y_1^2 + \lambda \varepsilon_1 + \mathcal{O}(r_1)$, and

$$\begin{aligned} r_3' &= r_3 F_3(r_3, y_3, \varepsilon_3), \\ y_3' &= \varepsilon_3 - y_3 F_3(r_3, y_3, \varepsilon_3) + \mathcal{O}(r_3), \\ \varepsilon_3' &= -2\varepsilon_3 F_3(r_3, y_3, \varepsilon_3), \end{aligned} \quad (2.16)$$

where $F_3(y_3, \varepsilon_3) = 1 - y_3^2 + \lambda \varepsilon_3 + \mathcal{O}(r_3)$. The $\mathcal{O}(r_i)$ -terms are of higher order, derived from \mathcal{R}_1 and \mathcal{R}_2 in the original equation (2.6). There are six equilibria on the invariant circle $\{r = \bar{\varepsilon} = 0\}$; see also Figure 2. We denote by

$$p_{a,1}^- = (0, -1, 0), \quad q_1^{\text{in}} = (0, 0, 0), \quad p_{a,1}^+ = (0, 1, 0) \quad (2.17)$$

the resulting equilibria in K_1 . The points $p_{a,1}^+$ and $p_{a,1}^-$ have a one-dimensional stable eigenspace along the y_1 -direction with eigenvalue -2 and a two-dimensional centre eigenspace. The point q_1^{in} is a saddle with eigenvalues $-1, 1, 2$. Similarly, we denote by

$$p_{r,3}^- = (0, -1, 0), \quad q_3^{\text{out}} = (0, 0, 0), \quad p_{r,3}^+ = (0, 1, 0) \quad (2.18)$$

the equilibria in K_3 . The points $p_{r,3}^+$ and $p_{r,3}^-$ have a one-dimensional unstable eigenspace along the y_3 -direction with eigenvalue 2 and a two-dimensional centre eigenspace. The point q_1^{out} is a saddle with eigenvalues 1, -1 , -2 . Note that we have two hyperbolic equilibria and four partially hyperbolic equilibria on $\{r = \bar{\varepsilon} = 0\}$ as opposed to complete lack of hyperbolicity in the original problem, see Figure 2.

The centre manifolds $M_{a,1}^\pm$ of $p_{a,1}^\pm$ in chart K_1 and $M_{r,3}^\pm$ of $p_{r,3}^\pm$ in chart K_3 are the unique extensions of slow manifolds $S_{a,1}^\pm$ and $S_{r,3}^\pm$, which correspond to $S_{a,\varepsilon}^\pm$ and $S_{r,\varepsilon}^\pm$ in the original coordinates. Furthermore, $M_{a,1}^\pm$ and $M_{r,3}^\pm$ correspond to locally invariant manifolds \bar{M}_a^\pm and \bar{M}_r^\pm of the blown-up vector field \bar{X} at the equilibria \bar{p}_a^\pm and \bar{p}_r^\pm . The idea is to track M_a^- as it moves across the sphere S^2 guided by the dynamics in chart K_2 . For that purpose, it is helpful to introduce the centre manifolds $N_{a,1}^\pm = M_{a,1}^\pm \cap \{r_1 = 0\}$ and $N_{r,3}^\pm = M_{r,3}^\pm \cap \{r_3 = 0\}$ and their global counterparts N_a^\pm and N_r^\pm . In that way, the dynamics can be analyzed first for $r = 0$, i.e. at the origin now blown up to a sphere where partial hyperbolicity is gained, and then for small $r > 0$ in order to connect the dynamics around the origin.

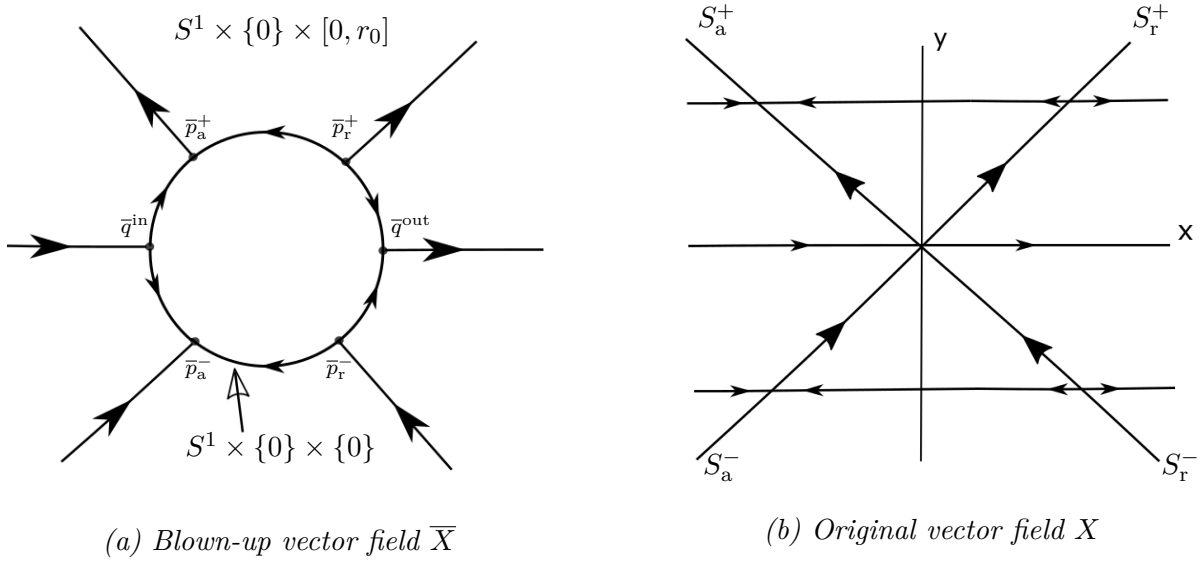


Figure 2: Blow-up at $(0,0,0)$ of equation (2.7). Figure 2 (b) shows a sketch of the original vector field X for $\varepsilon = 0$ and the four different branches of the critical manifold $S_a^-, S_r^-, S_a^+, S_r^+$. The arrows on the critical manifold indicate the direction of the reduced flow whereas the arrows on the y -fibres illustrate the layer flow. Figure 2 (a) sketches the blown-up vector field \bar{X} for $\varepsilon = 0$, i.e. on the submanifold $S^1 \times \{0\} \times [0, r_0]$. The figure illustrates the partially hyperbolic dynamics around the six equilibrium points on the invariant circle $S^1 \times \{0\} \times \{0\}$ which corresponds with the singularity at the origin in Figure 2 (b).

The crucial dynamics happen in the scaling chart K_2 . The desingularized equations have the form

$$\begin{aligned}
 x_2' &= x_2^2 - y_2^2 + \lambda + \mathcal{O}(r_2) \\
 y_2' &= 1 + \mathcal{O}(r_2) , \\
 r_2' &= 0 .
 \end{aligned}
 \tag{2.19}$$

Firstly, taking $r_2 = 0$, one can develop the typical behaviour of trajectories around the canard

case $\lambda = 1$. In this case, there is the solution $x_2 = y_2 = t$ denoted by $\gamma_2(t)$. We observe that

$$\lim_{t \rightarrow \infty} \kappa_{23}(\gamma_2(t)) = p_{r,3}^+, \quad \lim_{t \rightarrow -\infty} \kappa_{21}(\gamma_2(t)) = p_{a,1}^-.$$

Hence, for $\lambda = 1$, there is a connection between the equilibrium points \bar{p}_a^- and \bar{p}_r^+ by a trajectory $\bar{\gamma}$ which equals γ_2 in K_2 . Krupa and Szmolyan [15, Lemma 2.2] argue with the rotational property of (2.19) to observe that a connection from \bar{p}_a^- to \bar{p}_r^+ only exists for $\lambda = 1$. They conclude [15, Proposition 2.1] that for $\lambda < 1$ there is a unique trajectory connecting \bar{p}_a^- to \bar{p}_a^+ corresponding to \bar{N}_a^- , and for $\lambda > 1$ there is a unique trajectory connecting \bar{p}_a^- to \bar{q}^{out} corresponding to \bar{N}_a^- ; see Figure 2.

Moreover, one can argue that for $\lambda \neq 1$ the $\mathcal{O}(r_2)$ terms do not change the qualitative picture: if $\lambda < 1$, it follows from the previous considerations and perturbation theory that \bar{M}_a^- reaches the vicinity of \bar{M}_a^+ and that both centre manifolds are exponentially attracting. Analyzing the dynamics of (2.15) on \bar{M}_a^+ shows that the passage times near the equilibria \bar{p}_a^\pm are of order $\mathcal{O}(1/\varepsilon)$. Hence, one can conclude that the relevant contraction rate is of order $\mathcal{O}(e^{-C/\varepsilon})$ for some $C > 0$, as stated in Theorem 2.1.

If $\lambda > 1$, it follows from the previous considerations and perturbation theory that \bar{M}_a^- passes near \bar{q}^{out} . Contraction towards \bar{M}_a^- works as for $\lambda < 1$. The fact that $h(\varepsilon) = \mathcal{O}(\sqrt{\varepsilon})$ has to be worked out from the asymptotics of \bar{N}_a^- in chart K_2 and an analysis of the linearization of \bar{X} at \bar{q}^{out} in chart K_3 . The latter is delicate due to the resonance of the eigenvalues $-1, 1$ and 2 . Krupa and Szmolyan discuss this problem in detail for the fold singularity [14, Section 2.6] but not for the transcritical problem and claim that the statement follows analogously. We are going to give a detailed argument for the discrete-time problem below.

3 Transcritical singularity in discrete time

We can now turn to the main part, i.e., we want to analyze the discrete-time problem obtained via an explicit Euler method. For that purpose, we first set the higher order terms in (2.7), represented by \mathcal{R}_1 and \mathcal{R}_2 , to zero. We introduce the step size $h > 0$ of the Euler method as an additional variable and obtain a map $P : \mathbb{R}^4 \rightarrow \mathbb{R}^4$, whose iterations $P^n(z_0)$, for $n \in \mathbb{N}$ and $z_0 \in \mathbb{R}^4$, we are going to analyze close to the origin with $h, \varepsilon > 0$:

$$P : \begin{pmatrix} x \\ y \\ \varepsilon \\ h \end{pmatrix} \mapsto \begin{pmatrix} \tilde{x} \\ \tilde{y} \\ \tilde{\varepsilon} \\ \tilde{h} \end{pmatrix} = \begin{pmatrix} x + h(x^2 - y^2 + \lambda\varepsilon) \\ y + \varepsilon h \\ \varepsilon \\ h \end{pmatrix}. \quad (3.1)$$

Also in this case there is a normally hyperbolic critical manifold

$$S_0 = \{(x, y, \varepsilon, h) \in \mathbb{R}^4 : x^2 = y^2\} \setminus \{0\},$$

which splits into the attracting branches S_a^-, S_a^+ and repelling branches S_r^-, S_r^+ . It follows from [11, Theorem 4.1] that for $\varepsilon, h > 0$ small enough there are corresponding forward invariant slow manifolds $S_{a,\varepsilon,h}^-, S_{a,\varepsilon,h}^+$ and $S_{r,\varepsilon,h}^-, S_{r,\varepsilon,h}^+$. Note that $DP(0)$ only has quadruple eigenvalue 1, which means a complete loss of hyperbolicity at the origin, as in the ODE case.

Similarly to the problem in continuous time, we fix some $\rho > 0$ and let J be a small open interval around 0 in \mathbb{R} . We define

$$\Delta^{\text{in}} = \{(-\rho, y), y + \rho \in J\}, \quad \Delta_a^{\text{out}} = \{(-\rho, y), y - \rho \in J\}, \quad \Delta_e^{\text{out}} = \{(\rho, y), y \in J\},$$

where ε and h are fixed as prescribed by the map P ; see also Figure 3. In contrast with flows, the intervals $\Delta_a^{\text{out}}, \Delta_e^{\text{out}}$ are not necessarily hit by $P^n(-\rho, y)$ for fixed $y \in \Delta^{\text{in}}$ and some $n > 0$. Notice that we used an abbreviated notation $P^n(x, y, \varepsilon, h) = P^n(x, y)$ for the map P and also for points in Δ^{in} just denoting them by their y -coordinate. We define the transition maps from Δ^{in} to the vicinity of Δ_a^{out} and Δ_e^{out} by

$$\Pi_a(y) = P^{n^*(y)}(-\rho, y), \quad \text{where } n^*(y) = \arg \min_{n \in \mathbb{N}} \text{dist}(P^n(-\rho, y), \Delta_a^{\text{out}}), \quad y \in \Delta^{\text{in}}, \quad (3.2)$$

$$\Pi_e(y) = P^{m^*(y)}(-\rho, y), \quad \text{where } m^*(y) = \arg \min_{n \in \mathbb{N}} \text{dist}(P^n(-\rho, y), \Delta_e^{\text{out}}), \quad y \in \Delta^{\text{in}}. \quad (3.3)$$

We can formulate the main result on the transcritical singularity in discrete time (see Figure 3 for an illustration):

Theorem 3.1. *Fix $\lambda \neq 1$ and $\rho > 0$. There exists $\varepsilon_0 > 0$ such that the following assertions hold for all $\varepsilon \in [0, \varepsilon_0]$, $h > 0$ such that $0 < h\rho^3 < \varepsilon$ and any $0 < c < \rho h$.*

(T1) *If $\lambda < 1$, then the section Δ^{in} (including the point $\Delta^{\text{in}} \cap S_{a,\varepsilon,h}^-$) is mapped by Π_a to a set about $S_{a,\varepsilon,h}^+$ of y -width $\mathcal{O}\left((1-c)\frac{C\rho}{h\varepsilon}\right)$, where C is a positive constant, such that every point in $\Pi_a(\Delta^{\text{in}})$ is $\mathcal{O}(h\varepsilon)$ -close to Δ_a^{out} .*

(T2) *If $\lambda > 1$, then the manifold $S_{a,\varepsilon,h}^-$ passes through Δ_e^{out} at a point $(\rho, k(\varepsilon))$ where $k(\varepsilon) = \mathcal{O}(\varepsilon^{1/3})$. The section Δ^{in} is mapped by Π_e to a set about $S_{a,\varepsilon,h}^-$ of y -width $\mathcal{O}\left((1-c)\frac{C\rho}{h\varepsilon}\right)$, where C is a positive constant, such that every point in $\Pi_e(\Delta^{\text{in}})$ is $\mathcal{O}(h(\varepsilon + \rho^2))$ -close to Δ_e^{out} .*

Note carefully that Theorem 3.1 includes a precise requirement between three parameters, i.e., $0 < h\rho^3 < \varepsilon$, which means that the choice of step size for the Euler scheme is crucial. Since we only work in the normal form, the parameter ρ does not have to be small and can, for example, be chosen equal to 1 such that the requirement reads $0 < h < \varepsilon$. Our aim is to prove Theorem 3.1 using the blow-up method for the problem in four variables and to track individual trajectories inside the slow manifolds.

3.1 Blow-up transformation

We conduct the quasihomogeneous blow-up transformation

$$x = \bar{r}\bar{x}, \quad y = \bar{r}\bar{y}, \quad \varepsilon = \bar{r}^2\bar{\varepsilon}, \quad h = \bar{h}/\bar{r},$$

where $(\bar{x}, \bar{y}, \bar{\varepsilon}, \bar{h}, \bar{r}) \in B := S^2 \times (0, h_0] \times (0, \rho]$ for some $h_0, \rho > 0$. The change of variables in h is chosen such that the map is desingularized in the relevant charts. We exclude 0 from the domain of \bar{h} since at $\bar{h} = 0$ every point is a neutral fixed point. Due to the transformation $h = \bar{h}/\bar{r}$ we have to exclude 0 from the domain of \bar{r} as well.

The whole transformation can be formalised as a map $\Phi : B \rightarrow \mathbb{R}^4$. The map Φ induces a map \bar{P} on B by $\Phi \circ \bar{P} \circ \Phi^{-1} = P$. Analogously to the continuous time case, we are using the

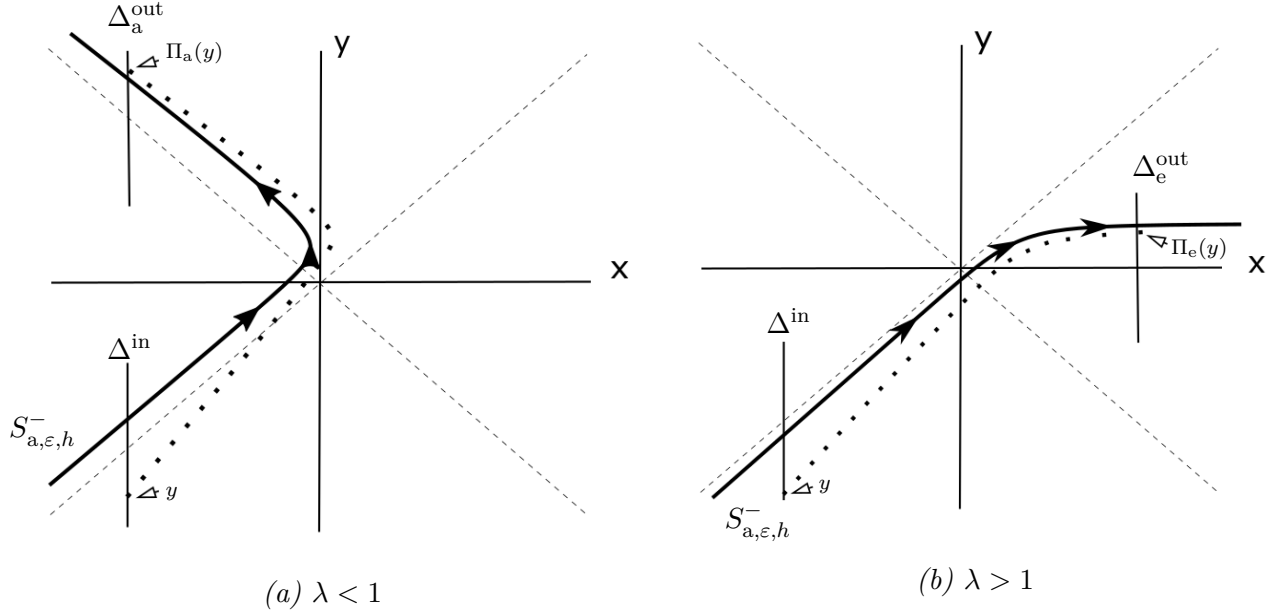


Figure 3: The sketches illustrate Theorem 3.1. For $\lambda < 1$ (Figure 3 (a)) and $\lambda > 1$ (Figure 3 (b)), the figures show the extension of the slow manifold $S_{a,\varepsilon,h}^-$ (black curve) for system (3.1) around the non-hyperbolic singularity at the origin and the trajectory of a point $y \in \Delta_a^{\text{in}}$ (dotted curve) to $\Pi_a(y)$ near Δ_a^{out} and to $\Pi_e(y)$ near Δ_e^{out} respectively. The dashed lines show the branches of the critical manifold S_0 .

charts K_i , $i = 1, 2, 3$, to describe the dynamics. The chart K_1 focuses on the entry of trajectories for any value of lambda and the exit of trajectories for $\lambda < 1$, and is given by

$$x = -r_1, \quad y = r_1 y_1, \quad \varepsilon = r_1^2 \varepsilon_1, \quad h = h_1 / r_1. \quad (3.4)$$

In the scaling chart K_2 the dynamics arbitrarily close to the origin are analyzed. It is given via the mapping

$$x = r_2 x_2, \quad y = r_2 y_2, \quad \varepsilon = r_2^2, \quad h = h_2 / r_2. \quad (3.5)$$

The exit chart K_3 plays a role for the dynamics emerging from a neighbourhood of the origin for $\lambda > 1$ and is given by

$$x = r_3, \quad y = r_3 y_3, \quad \varepsilon = r_3^2 \varepsilon_3, \quad h = h_3 / r_3. \quad (3.6)$$

There are four relevant changes of coordinates between the charts. The map $k_{12} : K_1 \rightarrow K_2$ is given by

$$x_2 = -\varepsilon_1^{-1/2}, \quad y_2 = \varepsilon_1^{-1/2} y_1, \quad r_2 = \varepsilon_1^{1/2} r_1, \quad h_2 = \varepsilon_1^{1/2} h_1, \quad (3.7)$$

$k_{21} : K_2 \rightarrow K_1$ is given by

$$\varepsilon_1 = x_2^{-2}, \quad y_1 = -x_2^{-1} y_2, \quad r_1 = -x_2 r_2, \quad h_1 = -x_2 h_2, \quad (3.8)$$

$k_{32} : K_3 \rightarrow K_2$ is given by

$$x_2 = \varepsilon_3^{-1/2}, \quad y_2 = \varepsilon_3^{-1/2} y_3, \quad r_2 = \varepsilon_3^{1/2} r_3, \quad h_2 = \varepsilon_3^{1/2} h_3, \quad (3.9)$$

and $k_{23} : K_2 \rightarrow K_3$ is given by

$$\varepsilon_3 = x_2^{-2}, \quad y_3 = x_2^{-1} y_2, \quad r_3 = x_2 r_2, \quad h_3 = x_2 h_2. \quad (3.10)$$

3.2 Dynamics in the chart K_1

We choose $\delta > 0$ small such that $|\lambda\delta| \leq 1$, to be determined later in more detail which will also determine $\varepsilon_0 = \rho^2\delta$. Furthermore, we assume $\nu := \rho h < \delta$ for fixed $h \in (0, h_0]$. We are interested in trajectories entering B at $\bar{r} = \rho$ which is best analyzed in the entering chart K_1 . At $\bar{r} = \rho$ we have $h_1 = \nu$. We investigate the dynamics within the domain

$$D_1 := \{(r_1, y_1, \varepsilon_1, h_1) \in \mathbb{R}^4 : r_1 \in [0, \rho], \varepsilon_1 \in [0, 2\delta], h_1 \in [0, \nu]\}.$$

Note that we have to bound h_1 from below since for $h_1 = 0$ everything is fixed and it is helpful to choose a uniform bound to get estimates on the contraction rates. A suitable choice is $h_1 \geq \nu/2$. The proportionality $h = h_1/r_1$ implies that $r_1 \geq \rho/2$. Furthermore, we want to see what happens for $\varepsilon_1 = \delta$. Due to the invariant relation $\varepsilon_1 r_1 h_1 = \varepsilon h$, this implies taking $\varepsilon_1 \geq \delta/4$. These considerations lead to introducing the subdomain $\hat{D}_1 \subset D_1$ which is given as

$$\hat{D}_1 := \{(r_1, y_1, \varepsilon_1, h_1) \in \mathbb{R}^4 : r_1 \in [\rho/2, \rho], \varepsilon_1 \in [\delta/4, \delta], h_1 \in [\nu/2, \nu]\}.$$

We will later restrict y_1 to obtain a small neighbourhood of Δ^{in} as entering domain. To derive the blown-up map we calculate

$$\begin{aligned} \tilde{r}_1 &= -\tilde{x} = -x - h(x^2 - y^2 + \lambda\varepsilon) \\ &= r_1 - \frac{h_1}{r_1}(r_1^2 - r_1^2 y_1^2 + \lambda r_1^2 \varepsilon_1) \\ &= r_1(1 - h_1(1 - y_1^2 + \lambda\varepsilon_1)). \end{aligned}$$

Similarly, we can derive the maps for the other variables in chart K_1 leading to the following dynamics, desingularised by choosing $h = h_1/r_1$:

$$\begin{aligned} \tilde{r}_1 &= r_1(1 - h_1 F_1(y_1, \varepsilon_1)), \\ \tilde{y}_1 &= (y_1 + \varepsilon_1 h_1)(1 - h_1 F_1(y_1, \varepsilon_1))^{-1}, \\ \tilde{\varepsilon}_1 &= \varepsilon_1(1 - h_1 F_1(y_1, \varepsilon_1))^{-2}, \\ \tilde{h}_1 &= h_1(1 - h_1 F_1(y_1, \varepsilon_1)), \end{aligned} \tag{3.11}$$

where $F_1(y_1, \varepsilon_1) = 1 - y_1^2 + \lambda\varepsilon_1$. Now we have to analyze the dynamics of (3.11) in detail. For any $h_1 \in [0, \nu]$ system (3.11) has the fixed points

$$v_{a,1}^-(h_1) = (0, -1, 0, h_1), \quad v_{a,1}^+(h_1) = (0, 1, 0, h_1).$$

The points $v_{a,1}^-$ and $v_{a,1}^+$ have a three-dimensional centre eigenspace and a one-dimensional eigenspace spanned by $(0, 1, 0, 0)^\top$ with the eigenvalue $\lambda_1 = 1 - 2h_1$, which is stable as long as $h_1 < 1$. Note that the set

$$\{w^{\text{in}}(h_1) := (0, 0, 0, h_1); h_1 \in [0, \nu]\}$$

is an invariant set for system (3.11) within D_1 . The points $w^{\text{in}}(h_1)$ have two stable and two unstable eigenvalues

$$\lambda_1 = 1 - 2h_1, \quad \lambda_2 = 1 - h_1, \quad \lambda_3 = (1 - h_1)^{-1}, \quad \lambda_4 = (1 - h_1)^{-2},$$

such that again the stability depends on h_1 and is analogous to the time-continuous case, if $h_1 < 1$. The eigenvalues λ_1, λ_2 correspond with the h_1 - and r_1 -directions and λ_3, λ_4 with the

y_1 -and ε_1 -directions. Moreover, we remark that we can re-interpret the stability conditions to obtain the same behaviour as in the continuous time case, such as

$$1 > |\lambda_1| = |1 - 2h_1|, \quad (3.12)$$

precisely as the stability criteria of the Euler method derived from the Dahlquist test equation [2] within each eigenspace of the continuous-time blow-up problem in chart K_1 .

We observe that the two-dimensional planes

$$S_{a,1}^\pm = \{(r_1, y_1, \varepsilon_1, h_1) \in D_1 : y_1 = \pm 1, \varepsilon_1 = 0\}$$

are invariant manifolds of D_1 only consisting of fixed points, attracting in the y_1 -direction and neutral in the other directions. One can extend these manifolds $S_{a,1}^\pm$ to center-stable invariant manifolds $M_{a,1}^\pm$ (see Figure 4), which are given in D_1 by graphs $y_1 = l_\pm(\varepsilon_1, h_1)$ for mappings l_\pm . We can derive l_\pm from the discrete invariance equation

$$l_\pm(\tilde{\varepsilon}_1, \tilde{h}_1) = \frac{l_\pm(\varepsilon_1, h_1) + \varepsilon_1 h_1}{1 - h_1 F_1(l_\pm(\varepsilon_1, h_1), \varepsilon_1)}. \quad (3.13)$$

Solving this equation allows us to make the following statement.

Proposition 3.2. *Equation (3.13) has the solutions*

$$l_-(\varepsilon_1, h_1) = -1 + \frac{1 - \lambda}{2} \varepsilon_1 + \mathcal{O}(\varepsilon_1^2 h_1), \quad (3.14)$$

$$l_+(\varepsilon_1, h_1) = 1 + \frac{1 + \lambda}{2} \varepsilon_1 + \mathcal{O}(\varepsilon_1^2 h_1). \quad (3.15)$$

which characterize $M_{a,1}^-$ and $M_{a,1}^+$ respectively. Furthermore, ε_1 is increasing on $M_{a,1}^-$ and decreasing on $M_{a,1}^+$, whereas h_1, r_1 are decreasing on $M_{a,1}^-$ and increasing on $M_{a,1}^+$.

Proof. It is easy to derive that for $l_-(\varepsilon_1, h_1)$ given by (3.14), we have

$$F_1(l_-(\varepsilon_1, h_1), \varepsilon_1) = \varepsilon_1 + \mathcal{O}(\varepsilon_1^2). \quad (3.16)$$

Hence, we observe that

$$\tilde{\varepsilon}_1 = \varepsilon_1 (1 - h_1 F_1(l_-(\varepsilon_1, h_1), \varepsilon_1))^{-2} = \varepsilon_1 + \mathcal{O}(\varepsilon_1^2 h_1)$$

and

$$\tilde{h}_1 = h_1 + \mathcal{O}(h_1^2 \varepsilon_1).$$

Therefore, we deduce that

$$\begin{aligned} \frac{l_-(\varepsilon_1, h_1) + \varepsilon_1 h_1}{1 - h_1 F_1(l_-(\varepsilon_1, h_1), \varepsilon_1)} &= (l_-(\varepsilon_1, h_1) + \varepsilon_1 h_1)(1 + h_1 \varepsilon_1 + \mathcal{O}(\varepsilon_1^2 h_1)) \\ &= l_-(\varepsilon_1, h_1) - h_1 \varepsilon_1 + \frac{1 - \lambda}{2} \varepsilon_1^2 h_1 + \varepsilon_1 h_1 + \mathcal{O}(\varepsilon_1^2 h_1) \\ &= l_-(\varepsilon_1, h_1) + \mathcal{O}(\varepsilon_1^2 h_1) = -1 + \frac{1 - \lambda}{2} \varepsilon_1 + \mathcal{O}(\varepsilon_1^2 h_1) = l_-(\tilde{\varepsilon}_1, \tilde{h}_1), \end{aligned}$$

which shows the claim for $l_-(\varepsilon_1, h_1)$. Since we can assume that $h_1 \varepsilon_1 < 1$, the dynamics on $M_{a,1}^-$ follow as stated. Similarly we can derive that for $l_+(\varepsilon_1, h_1)$ given by (3.15), we have

$$F_1(l_+(\varepsilon_1, h_1)) = -\varepsilon_1 + \mathcal{O}(\varepsilon_1^2).$$

The statements then follow analogously to before. \square

For all trajectories, as explained above, we have to consider the entry region

$$\Sigma_{1,-}^{\text{in}} := \{(r_1, y_1, \varepsilon_1, h_1) \in D_1 : r_1 = \rho, h_1 = \nu, \varepsilon_1 = \delta/4\}.$$

Before exiting \hat{D}_1 for the first time, the dynamics must reach the set

$$\Sigma_{1,-}^{\text{out}} = \left\{ (r_1, y_1, \varepsilon_1, h_1) \in \mathbb{R}^4 : \frac{\rho}{2} \leq r_1 \leq \frac{\rho}{2}(1 + \nu), \frac{\nu}{2} \leq h_1 \leq \frac{\nu}{2}(1 + \nu), \delta(1 - 2\nu) \leq \varepsilon_1 \leq \delta \right\},$$

since $F_1(y_1, \varepsilon_1) \leq 2$. Next, we want to find a set $R \subset \Sigma_{1,-}^{\text{in}}$ such that $M_{a,1}^- \cap \Sigma_{1,-}^{\text{in}} \subset R$ and there is a well-defined map $\Pi_{1,-} : R \rightarrow \Sigma_{1,-}^{\text{out}}$ that maps points in R along a trajectory of (3.11) to a first entry point in $\Sigma_{1,-}^{\text{out}}$. By Proposition 3.2, this is feasible for R small enough such that trajectories through R stay sufficiently close to $M_{a,1}^-$ in the first part of the passage in K_1 .

We choose R to be the interval

$$R_1 := \{(r_1, y_1, \varepsilon_1, h_1) \in \Sigma_{1,-}^{\text{in}}; -1 - \beta_1(\lambda) \leq y_1 \leq -1 + \hat{\beta}_1\} \quad (3.17)$$

with, for example,

$$\hat{\beta}_1 := |\lambda - 1| \delta, \quad \beta_1(\lambda) := \begin{cases} \frac{\lambda}{16} \delta & \text{if } 0 < \lambda < 1 \\ \frac{2\lambda-1}{16} \delta & \text{otherwise.} \end{cases} \quad (3.18)$$

Note that with these choices we have $M_{a,1}^- \cap \Sigma_{1,-}^{\text{in}} \subset R_1$ for ν, δ sufficiently small. Furthermore, these choices guarantee that the trajectories stay close to $M_{a,1}^-$ such that $F_1(y_1, \varepsilon_1)$ is positive, and, hence, we can formulate the following Proposition (see Figure 4).

Proposition 3.3. *Trajectories in \hat{D}_1 starting in R_1 are increasing in ε_1 and decreasing in h_1, r_1 . Hence, the transition map $\Pi_{1,-} : R_1 \rightarrow \Sigma_{1,-}^{\text{out}}$ is well-defined.*

Proof. It is enough to show that in this case $F_1(y_1, \varepsilon_1)$ is positive. If $\lambda \geq 1$ or $\lambda \leq 0$, we observe that $\beta_1(\lambda) = \frac{2\lambda-1}{16} \delta$ implies $F_1 \geq \frac{\delta - \mathcal{O}(\delta^2)}{8}$. If $0 < \lambda < 1$, we have

$$F_1(y_1, \varepsilon_1) \geq 1 - \left(-1 - \frac{\lambda}{16} \delta\right)^2 + \lambda \varepsilon_1 \geq \frac{\lambda}{8} \delta - \left(\frac{\lambda}{16}\right)^2 \delta^2.$$

Together with the considerations above, we can conclude the claim. \square

We can make the following statement about the transition time from R_1 to $\Sigma_{1,-}^{\text{out}}$ which will be crucial for estimates on the contraction close to $M_{a,1}^-$. Define $\gamma := 2|\lambda - 1| + |\lambda|$ and assume without loss of generality that $\nu < \frac{1}{8}$.

Lemma 3.4. *The transition time N of system (3.11) from a point $p = (\rho, y_1, \delta/4, \nu)$ in R_1 to the point $\Pi_{1,-}(p)$ in $\Sigma_{1,-}^{\text{out}}$ satisfies*

$$N \geq \frac{1}{17\gamma} \frac{1}{\nu\delta}.$$

Proof. Let $(\varepsilon_1(n))_{n \in \mathbb{N}}$ denote the trajectory starting at $\varepsilon_1(0) = \delta/4$ with

$$\varepsilon_1(n+1) = \varepsilon_1(n)(1 - h_1(n)F_1(y_1(n), \varepsilon_1(n)))^{-2}.$$

We can show by induction that for all $n \in \mathbb{N}$ such that $\varepsilon_1(n) \leq \delta$ we have

$$\varepsilon_1(n) \leq \frac{\delta}{4} + n(2\gamma\nu\delta^2 + f(\nu, \delta)), \quad (3.19)$$

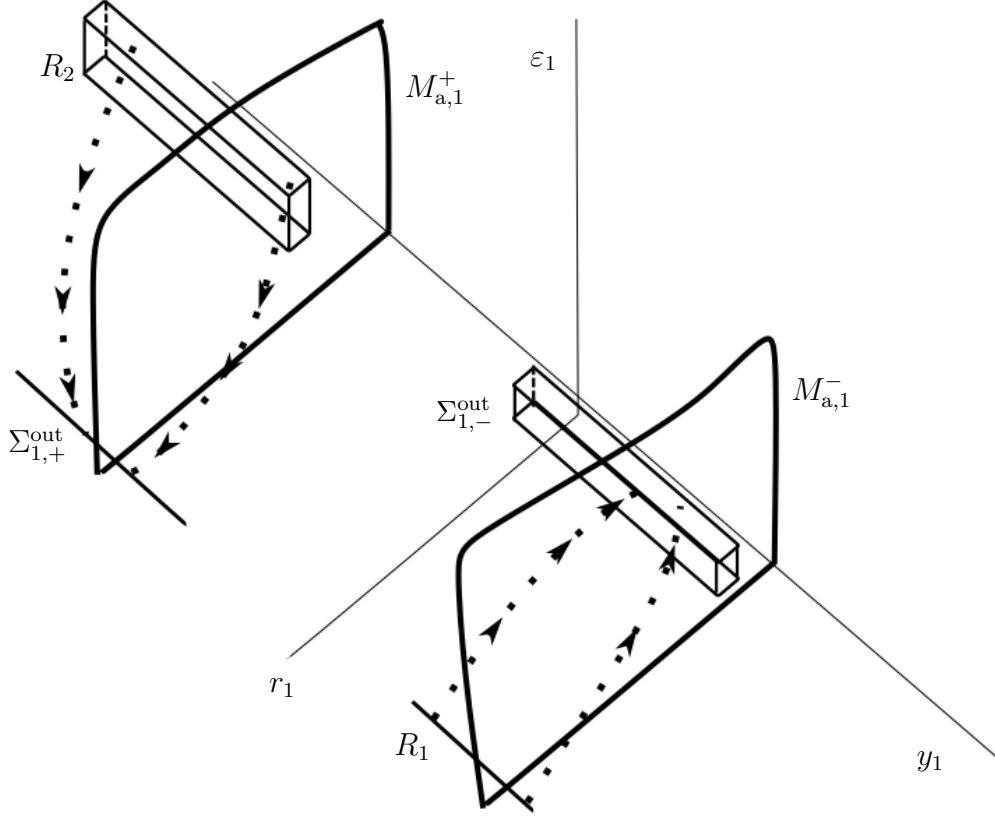


Figure 4: Illustration of the dynamics in chart K_1 in $(r_1, y_1, \varepsilon_1)$ -space. Note that, due to the relation $h_1 = r_1 h$, we can interpret $l_{\pm}(\varepsilon_1, h_1)$ as functions of (ε_1, r_1) and sketch its graphs, the center-stable manifolds $M_{a,1}^{\pm}$, as in the figure above. The figure shows trajectories (dotted lines) starting in R_1 up to reaching $\Sigma_{1,-}^{\text{out}}$ in the vicinity of $M_{a,1}^-$ and trajectories starting in R_2 up to reaching the vicinity of $\Sigma_{1,+}^{\text{out}}$ close to $M_{a,1}^+$.

where $f(\nu, \delta) = \mathcal{O}(\nu\delta^3)$ does not depend on n . In more detail, we observe that

$$\begin{aligned} h_1(n)F_1(y_1(n), \varepsilon_1(n)) &\leq h_1(n) \left[1 - (-1 + |\lambda - 1|\delta)^2 + \lambda\varepsilon_1(n) \right] \\ &\leq \nu \left[2|\lambda - 1|\delta + |\lambda|\delta - (\lambda - 1)^2\delta^2 \right] \\ &= \nu\gamma\delta - \nu(\lambda - 1)^2\delta^2. \end{aligned}$$

Hence, we conclude with a first order Taylor approximation that for some $g(\nu, \delta) = \mathcal{O}(\nu\delta^2)$ we have

$$\begin{aligned} \varepsilon_1(1) &\leq \frac{\delta}{4} (1 + \nu\gamma\delta + g(\nu, \delta))^2 = \frac{\delta}{4} + \frac{\gamma}{2}\nu\delta^2 + \frac{\delta}{4} (2g(\nu, \delta) + g(\nu, \delta)^2 + \nu^2\gamma^2\delta^2 + 2g(\nu, \delta)\nu\gamma\delta) \\ &\leq \frac{\delta}{4} + 2\gamma\nu\delta^2 + f(\nu, \delta), \end{aligned}$$

where $f(\nu, \delta) = \delta(2g(\nu, \delta) + \mathcal{O}(\nu^2\delta^2)) = \mathcal{O}(\nu\delta^3)$. Similarly, the step from n to $n + 1$ can be

written as

$$\begin{aligned}
\varepsilon_1(n+1) &\leq \varepsilon_1(n) (1 + \nu\gamma\delta + g(\nu, \delta))^2 \leq \varepsilon_1(n) + 2\gamma\nu\delta\varepsilon_1(n) + f(\nu, \delta), \\
&\leq \frac{\delta}{4} + n (2\gamma\nu\delta^2 + f(\nu, \delta)) + 2\gamma\nu\delta^2 + f(\nu, \delta), \\
&= \frac{\delta}{4} + (n+1) (2\gamma\nu\delta^2 + f(\nu, \delta)).
\end{aligned}$$

This shows (3.19) for all $n \in \mathbb{N}$ such that $\varepsilon_1(n) \leq \delta$. We can rewrite the right hand side of (3.19), using a geometric series, as

$$\frac{\delta}{4} + n (2\gamma\nu\delta^2 + f(\nu, \delta)) = \frac{\frac{\delta}{4}}{1 - n (8\gamma\nu\delta + \tilde{f}(\nu, \delta))},$$

where $\tilde{f}(\nu, \delta) = \mathcal{O}(\nu\delta^2)$. By definition of the transition time N we have $\varepsilon_1(N) \geq \delta(1 - 2\nu)$. Hence, we deduce that

$$\delta(1 - 2\nu) \leq \frac{\frac{\delta}{4}}{1 - N(8\gamma\nu\delta + \tilde{f}(\nu, \delta))},$$

and therefore

$$\delta \left(1 - 2\nu - \frac{1}{4}\right) \leq N\delta(1 - 2\nu)(8\gamma\nu\delta + \tilde{f}(\nu, \delta)).$$

Finally, for δ sufficiently small and due to $\nu < \frac{1}{8}$, this leads to

$$N \geq \frac{\frac{\delta}{2}}{\delta(1 - 2\nu)(8\gamma\nu\delta + \tilde{f}(\nu, \delta))} \geq \frac{1}{17\gamma\nu\delta},$$

which concludes the proof. \square

In addition to the first passage moving up the sphere, we already anticipate that for $\lambda < 1$ trajectories eventually re-enter K_1 from K_2 . With more precision to be added after the analysis in chart K_2 , we define

$$\begin{aligned}
\Sigma_{1,+}^{\text{in}} &:= \{(r_1, y_1, \varepsilon_1, h_1) \in D_1 : |\varepsilon_1 - \delta| \text{ small}, \left|r_1 - \frac{\rho}{2}\right| \text{ small}, \left|h_1 - \frac{\nu}{2}\right| \text{ small}\}, \\
\Sigma_{1,+}^{\text{out}} &:= \{(r_1, y_1, \varepsilon_1, h_1) \in D_1 : r_1 = \rho, h_1 = \nu, \varepsilon_1 = \delta/4, y_1 > 0\},
\end{aligned}$$

and denote by $\Pi_{1,+} : \Sigma_{1,+}^{\text{in}} \rightarrow \Sigma_{1,+}^{\text{out}}$ the map that sends points in $\Sigma_{1,+}^{\text{in}}$ along a trajectory of (3.11) to the point of this trajectory, which is closest to $\Sigma_{1,+}^{\text{out}}$. Note that $\Pi_{1,+}$ is well-defined sufficiently close to $M_{a,1}^+$ according to Proposition 3.2. In more detail, for β_1^+ and $\hat{\beta}_1^+$ to be determined more precisely in the analysis of chart K_2 , there is

$$R_2 := \{(r_1, y_1, \varepsilon_1, h_1) \in \Sigma_{1,+}^{\text{in}} ; 1 - \hat{\beta}_1^+ \leq y_1 \leq 1 + \beta_1^+\} \quad (3.20)$$

such that $M_{a,1}^+ \cap \Sigma_{1,+}^{\text{in}} \subset R_2$ and $\Pi_{1,+}$ is well-defined on R_2 ; see also Figure 4. Of course, a completely analogous result for the passage time as stated in Proposition 3.4 also holds for the map $\Pi_{1,+}$. We can use the lower bounds on the transition times to find the following lower bounds for the contraction rates of $\Pi_{1,-}|_{R_1}$ and $\Pi_{1,+}|_{R_2}$.

Proposition 3.5. *There are constants $K_1, K_2 > 0$ such that for any c with $0 < c < \nu = \rho h$*

1. *the map $\Pi_{1,-}|_{R_1}$ is a contraction (in the y_1 -direction) with a rate stronger than*

$$K_1(1-c)^{\frac{1}{17\gamma}\frac{1}{\nu\delta}}.$$

2. *the map $\Pi_{1,+}|_{R_2}$ is a contraction (in the y_1 -direction) with a rate stronger than*

$$K_2(1-c)^{\frac{1}{17\gamma}\frac{1}{\nu\delta}}.$$

Proof. The statement about $\Pi_{1,-}$ follows from Lemma 3.4 and the fact that the stable eigenvalue at the fixed points in $S_{a,1}^- \subset M_{a,1}^-$ is given by $1 - 2h_1 \geq 1 - \nu$, in combination with standard perturbation arguments.

The estimate for $\Pi_{1,+}$ uses the symmetry of system (3.11) with respect to the dynamics around $M_{a,1}^-$ and $M_{a,1}^+$: the transition time from $\Sigma_{1,+}^{\text{in}}$ to $\Sigma_{1,+}^{\text{out}}$ is of the same order as the transition time from $\Sigma_{1,-}^{\text{in}}$ to $\Sigma_{1,-}^{\text{out}}$, and the eigenvalues at $S_{a,1}^+$ are the same as at $S_{a,1}^-$. \square

3.3 Dynamics in the scaling chart K_2

We turn to analyzing the dynamics in the scaling chart K_2 in order to understand the behaviour of trajectories past the origin. The chart K_2 covers the upper part of the sphere, where we can desingularize with respect to ε . Recall from (3.7) that the change of coordinates from K_1 to K_2 is given by $k_{12} : K_1 \rightarrow K_2$ with

$$x_2 = -\varepsilon_1^{-1/2}, \quad y_2 = \varepsilon_1^{-1/2}y_1, \quad r_2 = \varepsilon_1^{1/2}r_1, \quad h_2 = \varepsilon_1^{1/2}h_1,$$

It becomes clear from this transformation that the set of interest can be restricted to

$$D_2 := \left\{ (x_2, y_2, r_2, h_2) \in \mathbb{R}^4 : \delta^{1/2}\frac{\rho}{2} \leq r_2 \leq \delta^{1/2}\rho, \delta^{1/2}\frac{\nu}{2} \leq h_2 \leq \delta^{1/2}\nu \right\}.$$

First of all, we need to make sure that $\kappa_{1,2}(\Pi_{1,-}(R_1)) \subset \Sigma_2^{\text{in}}$ for the entering set Σ_2^{in} . From the analysis in K_1 we derive that this is satisfied for

$$\Sigma_2^{\text{in}} := \left\{ (x_2, y_2, r_2, h_2) \in D_2 : -(\delta(1-2\nu))^{-1/2} \leq x_2 \leq -\delta^{-1/2}, \right. \\ \left. \delta^{-1/2}(-1 - \beta_2(\lambda)) \leq y_2 \leq \delta^{-1/2}(-1 + \hat{\beta}_2) \right\}, \quad (3.21)$$

where

$$\hat{\beta}_2 := |\lambda - 1|\delta, \quad \beta_2(\lambda) := \begin{cases} \frac{\lambda}{8}\delta & \text{if } 0 < \lambda < 1 \\ \frac{2\lambda-1}{4}\delta & \text{otherwise.} \end{cases} \quad (3.22)$$

We derive the desingularized equations and thereby justify the choice of blow-up in h . Observe that $\tilde{r}_2 = r_2$ since $\tilde{\varepsilon} = \varepsilon$ and $\varepsilon = r_2^2$. Similarly, we have $\tilde{h}_2 = h_2$. Furthermore observe that

$$\tilde{y}_2 = \frac{\tilde{y}}{\tilde{r}_2} = \frac{y + \varepsilon h}{\tilde{r}_2} = \frac{r_2 y_2 + r_2^2 h_2 r_2^{-1}}{r_2} = y_2 + h_2.$$

In addition to that, we obtain

$$\tilde{x}_2 = \frac{\tilde{x}}{\tilde{r}_2} = \frac{r_2 x_2 + h_2 r_2^{-1} (r_2^2 x_2^2 - r_2^2 y_2^2 + \lambda r_2^2)}{r_2} = x_2 + h_2 (x_2^2 - y_2^2 + \lambda).$$

Hence, summarising, the dynamics in chart K_2 are given by iterating the map

$$\begin{aligned}\tilde{x}_2 &= x_2 + h_2 (x_2^2 - y_2^2 + \lambda), \\ \tilde{y}_2 &= y_2 + h_2, \\ \tilde{r}_2 &= r_2, \\ \tilde{h}_2 &= h_2.\end{aligned}\tag{3.23}$$

The transition areas from K_2 to another chart depend on λ . For $\lambda < 1$, we will return to chart K_1 . Recall from (3.8) that the change of coordinates $k_{21} : K_2 \rightarrow K_1$ is given by

$$\varepsilon_1 = x_2^{-2}, \quad y_1 = -x_2^{-1} y_2, \quad r_1 = -x_2 r_2, \quad h_1 = -x_2 h_2,$$

We need to choose $\Sigma_{2,a}^{\text{out}}$ and the cuboid R_2 in $\Sigma_{1,+}^{\text{in}}$ in chart K_1 (see (3.20)) such that, firstly, trajectories starting in Σ_2^{in} reach $\Sigma_{2,a}^{\text{out}}$ and, secondly, $k_{21}(\Sigma_{2,a}^{\text{out}}) \subset R_2$. It turns out (see proof of Proposition 3.6 for the first criterion) that a suitable choice is given by

$$\Sigma_{2,a}^{\text{out}} := \left\{ (x_2, y_2, r_2, h_2) \in D_2 : -\delta^{-1/2} - \frac{h_2}{2} \leq x_2 \leq -\delta^{-1/2} + \frac{h_2}{2}, \right. \\ \left. \delta^{-1/2} (1 - \hat{\beta}_2^+) \leq y_2 \leq \delta^{-1/2} (1 + \beta_2^+) \right\}, \tag{3.24}$$

where we define $\beta_2^+ := \frac{|\lambda+1|}{2}\delta$ and $\hat{\beta}_2^+ := \frac{|\lambda+1|}{2}\delta$; see also Figure 5. The second criterion is then satisfied by adapting $\Sigma_{1,+}^{\text{in}}$ in the $(\varepsilon_1, r_1, h_1)$ -components accordingly via k_{21} and choosing, for example, $\beta_1^+ := \frac{3|\lambda+1|}{4}\delta$ and $\hat{\beta}_1^+ := \frac{3(|\lambda+1|)}{4}\delta$ in the definition of R_2 .

For $\lambda > 1$, we set the area of exit as

$$\Sigma_{2,e}^{\text{out}} := \{(x_2, y_2, r_2, h_2) \in D_2 : \delta^{-1/2} \leq x_2 \leq \delta^{-1/2} + h_2(\lambda + \delta^{-1}), \\ 0 \leq y_2 < \Omega(\lambda)\delta^{-1/6}\}, \tag{3.25}$$

where $\Omega(\lambda) > 0$ is a constant for fixed λ ; see also Figure 5. In the situation of continuous time, the y_2 -component in $\Sigma_{2,e}^{\text{out}}$ can be bounded by a constant independent from δ , by using the Riccati equation [14, Proposition 2.3]. As we do not have such a tool in the case of maps, we give an estimate from a first order expansion in h of the iterated maps (see proof of Proposition 3.6).

Let us denote the sequence induced by iterating (3.23) for some initial condition (x_0, y_0) as $(x_2(n), y_2(n))$ for $n \in \mathbb{N}$, and call such a sequence a trajectory. As for continuous time, the special case is the canard problem, i.e. when $\lambda = 1$. In this case, for any $c = x_0 = y_0 \in \mathbb{R}$ the system of maps has the obvious solution $\gamma_2^c(n)$ with $x_2(n) = y_2(n) = c + nh_2$. For $\lambda \neq 1$ we can make the following direct observations about the dynamics of the maps, where we recall that $\nu := \rho h < \delta$, in particular $\nu < \frac{1}{8}$.

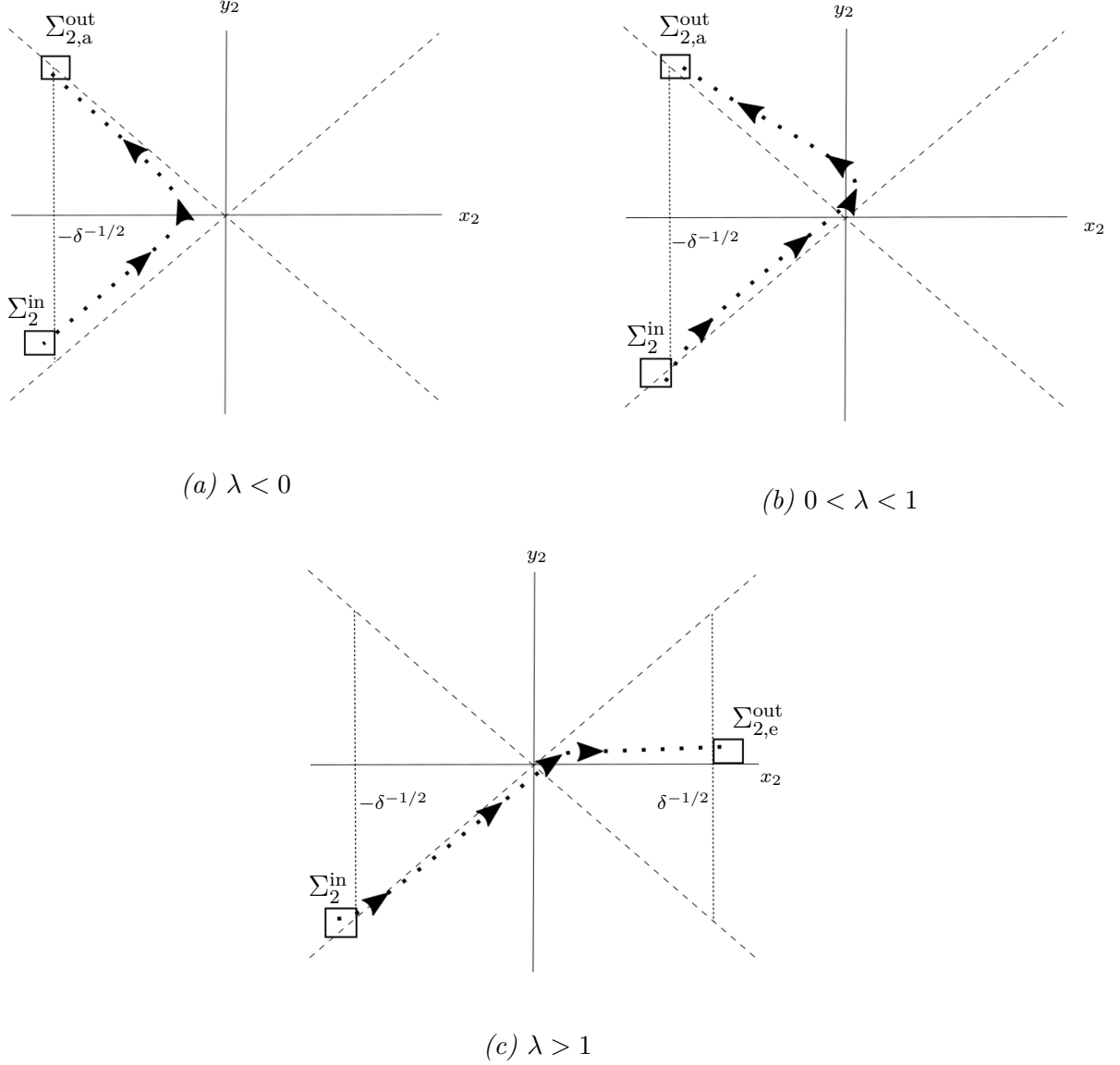


Figure 5: Typical trajectories (dotted lines) in the K_2 chart, i.e. solutions of (3.23) starting in Σ_2^{in} for different values of λ , as ascertained in the proof of Proposition 3.6. For $\lambda < 0$ (a) the y_2 -axis is not crossed, as opposed to the case $0 < \lambda < 1$ (b), but in both situations the rectangle $\Sigma_{2,a}^{\text{out}}$ is reached close to the diagonal (dashed lines), specifically $(x_2, y_2) = (-\delta^{-1/2}, -\delta^{-1/2})$. For $\lambda > 1$ (c), trajectories reach the rectangle $\Sigma_{2,e}^{\text{out}}$ close to $\{x_2 = \delta^{-1/2}\}$ above the x_2 -axis.

Proposition 3.6. *The following results hold:*

(P1) *If $\lambda < 1$, every trajectory starting in Σ_2^{in} passes through $\Sigma_{2,a}^{\text{out}}$.*

(P2) *If $\lambda > 1$, every trajectory starting in Σ_2^{in} passes through $\Sigma_{2,e}^{\text{out}}$.*

The proof of this proposition is based on a couple of lemmas, which are shown in the following. We divide the diagonals $\{x = y\}$ and $\{x = -y\}$ into the subsets

$$S_{a,2}^- := \{(x, y) \in \mathbb{R}^2 : y \leq 0, x = y\}, \quad S_{a,2}^+ := \{(x, y) \in \mathbb{R}^2 : y \geq 0, x = -y\}$$

and

$$S_{r,2}^- := \{(x, y) \in \mathbb{R}^2 : y \leq 0, x = -y\}, \quad S_{r,2}^+ := \{(x, y) \in \mathbb{R}^2 : y \geq 0, x = y\}.$$

Furthermore, we write as a shorthand $x_{2,n} = x_2(n), y_{2,n} = y_2(n)$ for $n \in \mathbb{N}$ and investigate the behaviour of the trajectories

$$\begin{aligned} y_{2,n+1} &= y_{2,n} + h_2, \\ x_{2,n+1} &= x_{2,n} + h_2\lambda + h_2(x_{2,n}^2 - y_{2,n}^2) \end{aligned}$$

for different values of λ . In fact, even for $\lambda < 1$, there are subtle differences in the paths of trajectories (see Figure 5).

Lemma 3.7. *The following cases occur for $\lambda < 1$:*

- *Let $0 < \lambda < 1$ and δ be sufficiently small. Then any trajectory starting in Σ_2^{in} is strictly increasing in x as long as $x_{2,n}, y_{2,n} < 0$, and will be above the diagonal $\{x = y\}$ at a certain point of time and stay there forever afterwards. In particular, if $(x_{2,0}, y_{2,0})$ in Σ_2^{in} with $y_{2,0} < x_{2,0} < 0$, there exists $n^* \in \mathbb{N}$ such that $x_{2,n^*} \leq y_{2,n^*} < 0$ and*

$$\frac{n^* h_2}{n^* h_2 + \frac{\delta^{1/2}}{8}} \geq \lambda.$$

- *If $\lambda \leq 0$, any trajectory starting in Σ_2^{in} is strictly increasing in x as long as $x_{2,n}, y_{2,n} < 0$ and will be above the diagonal $\{x = y\}$ at any point of time.*

Proof. We start with the case $0 < \lambda < 1$. Consider an initial condition $(x_{2,0}, y_{2,0})$ in Σ_2^{in} with $y_{2,0} < x_{2,0} < 0$, i.e., below $S_{a,2}^-$. We obviously have $x_{2,1} < x_{2,0} + \lambda h_2$. Furthermore, observe that

$$\begin{aligned} x_{2,0}^2 - y_{2,0}^2 + \lambda &\geq \delta^{-1} - (\delta^{-1/2}(-1 - \beta_2(\lambda)))^2 + \lambda \\ &= \delta^{-1} - \delta^{-1} - \frac{1}{4}\lambda - \frac{1}{64}\lambda^2\delta + \lambda \\ &= \frac{3}{4}\lambda - \frac{1}{64}\lambda^2\delta \geq \frac{1}{2}\lambda. \end{aligned}$$

Hence, $x_{2,1} \geq x_{2,0} + \frac{\lambda}{2}h_2$. Either we already have $x_{2,1} \leq y_{2,1} < 0$. If not, we can infer from the facts $0 > y_{2,1} > y_{2,0}$, $0 > x_{2,1} > x_{2,0}$ and $x_{2,1} - y_{2,1} < x_{2,0} - y_{2,0}$ that $y_{2,1}^2 - x_{2,1}^2 < y_{2,0}^2 - x_{2,0}^2$. Hence, we have $x_{2,0} + \lambda h_2 < x_{2,2} < x_{2,0} + 2\lambda h_2$ and obviously $y_{2,2} = y_{2,0} + 2h_2$. Therefore, we see inductively that for $0 > x_{2,n} > y_{2,n}$ both sequences are increasing and we either already have $x_{2,n+1} \leq y_{2,n+1} < 0$ or

$$\begin{aligned} x_{2,n+1} - y_{2,n+1} &< x_{2,0} - y_{2,0} - (n+1)(1-\lambda)h_2 < \frac{\lambda}{8}\delta^{1/2} - (n+1)(1-\lambda)h_2 \\ &= \lambda \left((n+1)h_2 + \frac{\delta^{1/2}}{8} \right) - (n+1)h_2. \end{aligned}$$

Thus, we can conclude that $x_{2,n^*} \leq y_{2,n^*} < 0$ for some n^* such that $\lambda \leq \frac{n^* h_2}{n^* h_2 + \frac{\delta^{1/2}}{8}}$, if δ is chosen small enough such that $\frac{\delta^{-1/2}}{\delta^{-1/2} + \frac{\delta^{1/2}}{8}} > \lambda$. Namely, if there was $\hat{n} \in \mathbb{N}$ such that $0 > x_{2,n} > y_{2,n}$ for all $n < \hat{n}$ and $x_{2,\hat{n}} > 0$, we would have, for h_2, δ small enough, that $\frac{\hat{n}-1}{\hat{n}} \geq \lambda$ and would obtain

$$\frac{(\hat{n}-1)h_2}{(\hat{n}-1)h_2 + \frac{\delta^{1/2}}{8}} \geq \frac{\lambda \hat{n} h_2}{\lambda \hat{n} h_2 + \frac{\delta^{1/2}}{8}} > \frac{\delta^{-1/2}}{\delta^{-1/2} + \frac{\delta^{1/2}}{8}} > \lambda,$$

which is a contradiction, since this would imply $x_{2,\hat{n}-1} < y_{2,\hat{n}-1}$ with the above.

Assume now that, at time $n \in \mathbb{N}$, the trajectory is above the diagonal $\{x = y\}$, i.e., $x_{2,n} \leq y_{2,n}$. In particular, this covers the case when $x_{2,n} \leq y_{2,n} < 0$, when the trajectory lies above $S_{a,2}^-$, which is relevant for the initial data. We have $y_{2,n+1} = y_{2,n} + h_2$ and $x_{2,n+1} \geq x_{2,n} + h_2\lambda$. If $x_{2,n} = y_{2,n}$, then obviously $x_{2,n+1} < y_{2,n+1}$. If $x_{2,n} < y_{2,n}$, we observe that

$$x_{2,n+1} \geq y_{2,n+1} \quad \text{iff} \quad 1 + \frac{h_2(1-\lambda)}{y_{2,n} - x_{2,n}} \leq -h_2(x_{2,n} + y_{2,n}). \quad (3.26)$$

Hence, since $h_2|x_{2,n} + y_{2,n}| < 2(1-2\nu)^{-1/2}\delta^{-1/2}\delta^{1/2}\nu < 1$, we have $x_{2,n+1} < y_{2,n+1}$ and the argument goes on inductively. We can also see that, for $x_{2,n} \leq y_{2,n} < 0$, the trajectories stay close to $S_{a,2}^-$ since, if $x_{2,n}^2 - y_{2,n}^2 > 1 - \lambda$, we have that $y_{2,n+1} - x_{2,n+1} < y_{2,n} - x_{2,n}$. This concludes the proof of the first statement.

Next, we consider the case $\lambda \leq 0$. Again, assume that at time $n \in \mathbb{N}$ the trajectory is above the diagonal $\{x = y\}$, i.e. $x_{2,n} \leq y_{2,n}$. In particular, this covers the case when $x_{2,n} \leq y_{2,n} < 0$ as relevant for the initial data. If $x_{2,n} = y_{2,n}$, then obviously $x_{2,n+1} < y_{2,n+1}$. If $x_{2,n} < y_{2,n}$, we observe as before that (3.26) holds and that $h_2|x_{2,n} + y_{2,n}| < 1$. Hence, we have $x_{2,n+1} < y_{2,n+1}$ and the argument goes on inductively. Therefore trajectories stay above the diagonal. Furthermore, observe that $y_{2,0}^2 \leq \left(\delta^{-1/2} \left(-1 - \frac{2\lambda-1}{4}\delta\right)\right)^2$ and therefore

$$x_{2,0}^2 - y_{2,0}^2 + \lambda \geq \delta^{-1} - \delta^{-1} - \lambda + \frac{1}{2} - \frac{(2\lambda-1)^2}{16}\delta + \lambda = \frac{1}{2} - \frac{(2\lambda-1)^2}{16}\delta,$$

which is greater than 0 for δ small enough, depending on λ . Hence, $x_{2,1} > x_{2,0}$. We show that $x_{2,n+1} > x_{2,n}$ as long as $x_{2,n} < y_{2,n} < 0$ by proving that $\xi_n := x_{2,n}^2 - y_{2,n}^2 + \lambda > 0$ implies $x_{2,n+1}^2 - y_{2,n+1}^2 + \lambda > 0$. Assuming that $x_{2,n} < y_{2,n} < 0$ and $\xi_n > 0$ yields

$$\begin{aligned} x_{2,n+1}^2 - y_{2,n+1}^2 + \lambda &= (x_{2,n} + h_2\xi_n)^2 - (y_{2,n} + h_2)^2 + \lambda \\ &= \xi_n + h_2^2(\xi_n^2 - 1) + 2h_2(|y_{2,n}| - \xi_n|x_{2,n}|). \end{aligned}$$

From there, it is easy to observe that for h_2 small enough the claim follows. \square

Although the argument is quite technical, the proof of the last lemma shows that the key steps in the scaling chart involve the sign of the nonlinear term for the x_2 -variable. This idea can also be carried out in the case $\lambda > 1$.

Lemma 3.8. *Let $\lambda > 1$ and δ, ν sufficiently small. Then all trajectories starting in Σ_2^{in} are strictly increasing in x as long as $x_{2,n}, y_{2,n} < 0$, will be below the diagonal $\{x = y\}$ at a certain point of time and stay there forever afterwards. In particular, if $(x_{2,0}, y_{2,0})$ in Σ_2^{in} with $x_{2,0} < y_{2,0} < 0$, there is a $n^* \in \mathbb{N}$ such that $y_{2,n^*} \leq x_{2,n^*} < 0$ and*

$$n^*h_2 \geq \delta^{1/2}.$$

Proof. We consider two cases, trajectories below and above the diagonal. First, we assume that, at time $n \in \mathbb{N}$, the trajectory is below the diagonal $\{x = y\}$ so that $y_{2,n} \leq x_{2,n}$. In particular, this covers the case when $y_{2,n} \leq x_{2,n} < 0$, i.e., the trajectory lies below $S_{a,2}^-$, which is relevant for the initial data. If $x_{2,n} = y_{2,n}$, then obviously $y_{2,n+1} < x_{2,n+1}$. If $y_{2,n} < x_{2,n}$, we observe similarly to (3.26) that

$$y_{2,n+1} \geq x_{2,n+1} \quad \text{iff} \quad 1 + \frac{h_2(\lambda-1)}{x_{2,n} - y_{2,n}} \leq -h_2(x_{2,n} + y_{2,n}).$$

Hence, since $h_2 |x_{2,n} + y_{2,n}| < (2(1 - 2\nu)^{-1/2} \delta^{-1/2} + \frac{2\lambda-1}{4} \delta^{1/2}) \delta^{1/2} \nu < 1$ due to $\delta\lambda \leq 1$ and $\nu < \frac{1}{8}$, we have $y_{2,n+1} < x_{2,n+1}$ and the argument goes on inductively.

Moreover, we check that the sequences are increasing in this case. We consider an initial condition $(x_{2,0}, y_{2,0})$ in Σ_2^{in} with $y_{2,0} < x_{2,0} < 0$, i.e., below $S_{a,2}^-$. We obviously have $x_{2,1} < x_{2,0} + \lambda h_2$. Furthermore, observe that

$$\begin{aligned} x_{2,0}^2 - y_{2,0}^2 + \lambda &\geq \delta^{-1} - (\delta^{-1/2}(-1 - \beta_2(\lambda)))^2 + \lambda \\ &= \delta^{-1} - \delta^{-1} - \lambda + \frac{1}{2} - \frac{(2\lambda - 1)^2}{16} \delta + \lambda \\ &= \frac{1}{2} - \frac{(2\lambda - 1)^2}{16} \delta \geq \frac{1}{4}, \end{aligned}$$

if δ is chosen sufficiently small in comparison to λ . Hence, $x_{2,1} \geq x_{2,0} + \frac{1}{4}h_2$. Note in particular that if $y_{2,0} = \delta^{-1/2}(-1 - \beta_2(\lambda)) =: y^*$, we have $x_{2,0}^2 - y_{2,0}^2 + \lambda < \frac{1}{2}$. From here, it is easy to observe that, for ν small enough, $x_{2,1} - y_{2,1} < x_{2,0} - y^*$. This together with the fact that $|y_{2,1} + x_{2,1}| < |y_{2,0} + x_{2,0}|$ yields $x_{2,1}^2 - y_{2,1}^2 + \lambda > \frac{1}{4}$. Hence, we have $x_{2,2} \geq \frac{1}{2}h_2$ and obviously $y_{2,2} = y_{2,0} + 2h_2$. Therefore, we see inductively that for $0 > x_{2,n} > y_{2,n}$ both sequences are increasing.

As the second case, we consider a trajectory with initial condition $(x_{2,0}, y_{2,0})$ in Σ_2^{in} and $x_{2,0} < y_{2,0} < 0$, i.e., above $S_{a,2}^-$. Either we already have $y_{2,1} \leq x_{2,1} < 0$. If not, we have $x_{2,1} > x_{2,0} + \lambda h_2$ and obviously $y_{2,1} = y_{2,0} + h_2$. Therefore, we see inductively that for $x_{2,n} < y_{2,n} < 0$ both sequences are increasing and we either already have $y_{2,n+1} \leq x_{2,n+1} < 0$ or

$$\begin{aligned} x_{2,n+1} - y_{2,n+1} &> x_{2,0} - y_{2,0} + (n+1)(\lambda - 1)h_2 \\ &\geq \delta^{-1/2} - \delta^{-1/2}(1 - 2\nu)^{-1/2} - (\lambda - 1)\delta^{1/2} + (n+1)(\lambda - 1)h_2. \end{aligned}$$

Thus, we can conclude that $y_{2,n^*} \leq x_{2,n^*} < 0$ for some n^* such that $n^*h \geq \delta^{1/2} \left(1 + \frac{(1-2\nu)^{-1/2}-1}{\lambda-1}\right)$. Using $(1 - 2\nu)^{-1/2} > 1$, the claim follows. \square

Finally, we turn to the proof of Proposition 3.6.

Proof of Proposition 3.6. We distinguish three cases: (I) $0 < \lambda < 1$, (II) $\lambda \leq 0$, and (III) $\lambda > 1$. The case distinction is going to allow us to apply each of the preliminary results obtained above.

Case (I) $0 < \lambda < 1$: From Lemma 3.7 we know that trajectories starting in Σ_2^{in} will be above the diagonal $\{x = y\}$ at certain point of time and stay there forever afterwards. From this result and the fact that $y_{2,n}$ and $x_{2,n}$ are both strictly increasing uniformly as long as $|y_{2,n}| \leq |x_{2,n}|$, we can conclude that any such trajectory reaches a point $(x_{2,\tilde{n}}, y_{2,\tilde{n}})$, with $y_{2,\tilde{n}} > 0$, such that $y_{2,\tilde{n}}^2 > x_{2,\tilde{n}}^2$. We can conclude that there must be a minimal $n^* > \tilde{n}$ such that $y_{2,n^*}^2 > x_{2,n^*}^2 + \lambda$. Note that (x_{2,n^*}, y_{2,n^*}) lies between $S_{a,2}^+$ and $S_{r,2}^+$. As long as this is the case for $n > n^*$, we have $x_{2,n+1} < x_{2,n}$. Additionally, we observe that for $y_{2,n}^2 - x_{2,n}^2 > \lambda + 1$ we have $y_{2,n+1} + x_{2,n+1} < y_{2,n} + x_{2,n}$. Hence, trajectories are rapidly approaching the vicinity of $S_{2,a}^+$. Similarly to (3.26), we find that for any such $y_{2,n} > -x_{2,n} > 0$

$$|x_{2,n+1}| \geq y_{2,n+1} \quad \text{iff} \quad 1 + \frac{h_2(1 + \lambda)}{y_{2,n} - |x_{2,n}|} \leq h_2(|x_{2,n}| + y_{2,n}).$$

Hence, since $h_2 |x_{2,n}| + y_{2,n} < (2 + \delta + h_2)\nu < 1$ before hitting $\Sigma_{2,a}^{\text{out}}$, we have $|x_{2,n+1}| < y_{2,n+1}$ and the argument goes on inductively before hitting $\Sigma_{2,a}^{\text{out}}$. The fact that the trajectory will actually

be located within $\Sigma_{2,a}^{\text{out}}$ at a certain point of time can be inferred as follows: we observe from the above that $(x_{2,n}, y_{2,n})$ satisfies $0 \leq y_{2,n}^2 - x_{2,n}^2 \leq \lambda + 1$ for large enough n . First, we can conclude that $x_{2,n} - x_{2,n+1} \leq h_2$. Hence, there is an $m \in \mathbb{N}$ such that $x_{2,m} \in [-\delta^{-1/2} - \frac{h_2}{2}, -\delta^{-1/2} + \frac{h_2}{2}]$. Therefore we have $y_{2,m} \geq \delta^{-1/2} - \frac{h_2}{2}$ and

$$y_{2,m}^2 \leq \delta^{-1} + (\lambda + 1) - h_2\delta^{-1/2} + \frac{h_2^2}{4} \leq \delta^{-1} + 2\beta_2^+\delta^{-1} + \delta^{-1}(\beta_2^+)^2 = \left(\delta^{-1/2}(1 + \beta_2^+)\right)^2.$$

Figure 5 (b) illustrates the behaviour of trajectories starting in $\Sigma_{2,a}^{\text{in}}$ for $0 < \lambda < 1$.

Case (II) $\lambda \leq 0$: We know from Lemma 3.7 that any trajectory starting in Σ_2^{in} is strictly increasing in x as long as $x_{2,n}, y_{2,n} < 0$ and will be above the diagonal $\{x = y\}$ at any point of time. Analogously to before, we can conclude that there exists a minimal $n^* \in \mathbb{N}$ such that $y_{2,n^*} > 0$ and $y_{2,n^*}^2 > x_{2,n^*}^2 + \lambda$. Note that if (x_{2,n^*}, y_{2,n^*}) lies between $S_{a,2}^+$ and $S_{r,2}^+$ and stays in this region for all $n > n^*$ before hitting $\Sigma_{a,2}^{\text{out}}$, as for example for $-1 \leq \lambda \leq 0$, the arguments go exactly as before. Otherwise we observe, symmetrically to before, that $(x_{2,n}, y_{2,n})$ satisfies $0 \geq x_{2,n}^2 - y_{2,n}^2 + \lambda \geq -1$ for large enough n . Again, we infer that $x_{2,n} - x_{2,n+1} \leq h_2$ and conclude that there is an $m \in \mathbb{N}$ such that $x_{2,m} \in [-\delta^{-1/2} - \frac{h_2}{2}, -\delta^{-1/2} + \frac{h_2}{2}]$. Therefore we have $y_{2,m} \leq \delta^{-1/2} + \frac{h_2}{2}$ and for δ sufficiently small depending on λ

$$y_{2,m}^2 \geq \delta^{-1} - h_2\delta^{-1/2} + \frac{h_2^2}{4} + \lambda \geq \delta^{-1} + \lambda + \frac{(|\lambda| + 1)^2}{4}\delta - 1 = \left(\delta^{-1/2}(1 - \hat{\beta}_2^+)\right)^2.$$

Figure 5 (a) illustrates the behaviour of trajectories starting in $\Sigma_{2,a}^{\text{in}}$ for $\lambda < 0$.

Case (III) $\lambda > 1$: We can conclude from Lemma 3.8 that trajectories starting in Σ_2^{in} will be below $S_{a,2}^-$ at a certain point of time and stay below the diagonal $\{x = y\}$ forever afterwards. From that and the fact that $y_{2,n}$ is strictly increasing for all time, we can conclude that any such trajectory will reach a point (x_{2,n^*}, y_{2,n^*}) with $x_{2,n^*} > y_{2,n^*} > 0$. Then the trajectory will increase its distance from the diagonal in each time step by

$$h_2(\lambda - 1) + h_2(x_{2,n}^2 - y_{2,n}^2).$$

Let us take the largest n such that $x_{2,n} > 0 \geq y_{2,n}$. It is now obvious that there is an $m \in \mathbb{N}$ such that $\delta^{-1/2} \leq x_{2,n+m} \leq \delta^{-1/2} + h_2(\lambda + \delta^{-1})$. We give an upper bound for $y_{2,m+n}$ by expanding x_n up to h_2^3 , which is the first order estimate in this case:

$$\begin{aligned} (1 + 2\nu)\delta^{-1/2} &\geq x_{2,m+n} > mh_2\lambda + \left(\sum_{k=1}^{m-1} k^2\right) (\lambda^2 - 1)h_2^3 \\ &\geq y_{2,m+n}\lambda + \frac{1}{6}(\lambda^2 - 1)y_{2,m+n}(y_{2,m+n} - h_2)(2y_{2,m+n} - h_2) \\ &\geq \lambda y_{2,m+n} + \frac{1}{6}(\lambda^2 - 1)y_{2,m+n}^3. \end{aligned}$$

Hence, we conclude that $y_{2,m+n} = \mathcal{O}(\delta^{-1/6})$ and $(x_{2,n+m}, y_{2,m+n}) \in \Sigma_{2,e}^{\text{out}}$. Figure 5 (c) illustrates such a trajectory. \square

3.4 Dynamics in the chart K_3

We investigate the dynamics in the chart K_3 (2.10) for $\lambda > 1$. First, recall from (3.10) that the change of coordinates $k_{23} : K_2 \rightarrow K_3$ is given by

$$\varepsilon_3 = x_2^{-2}, \quad y_3 = x_2^{-1}y_2, \quad r_3 = x_2r_2, \quad h_3 = x_2h_2,$$

Symmetrically to the chart K_1 , we define

$$D_3 := \{(r_3, y_3, \varepsilon_3, h_3) \in \mathbb{R}^4 : r_3 \in [0, \rho], \varepsilon_3 \in [0, \delta], h_3 \in [0, \nu]\}$$

and

$$\hat{D}_3 := \{(r_3, y_3, \varepsilon_3, h_3) \in \mathbb{R}^4 : r_3 \in [\rho/2, \rho], \varepsilon_3 \in [\delta/4, \delta], h_3 \in [\nu/2, \nu]\}.$$

Since we need to have $k_{23}(\Sigma_{2,e}^{\text{out}}) \subset \Sigma_3^{\text{in}}$, a suitable choice is given by

$$\Sigma_3^{\text{in}} := \{(r_3, y_3, \varepsilon_3, h_3) \in D_3 : (\delta^{-1} + 4\nu\delta^{-1})^{-1} \leq \varepsilon_3 \leq \delta\}.$$

Furthermore, we will simply set

$$\Sigma_3^{\text{out}} := \{(r_3, y_3, \varepsilon_3, h_3) \in D_3 : r_3 = \rho, h_3 = \nu, \varepsilon_3 = \delta/4, y_3 > 0\},$$

and will end the analysis with the point of the trajectory which is closest to Σ_3^{out} . The dynamics, desingularised by choosing $h = h_3/r_3$, look as follows:

$$\begin{aligned} \tilde{r}_3 &= r_3(1 + h_3 F_3(y_3, \varepsilon_3)), \\ \tilde{y}_3 &= (y_3 + \varepsilon_3 h_3)(1 + h_3 F_3(y_3, \varepsilon_3))^{-1} \\ \tilde{\varepsilon}_3 &= \varepsilon_3(1 + h_3 F_3(y_3, \varepsilon_3))^{-2} \\ \tilde{h}_3 &= h_3(1 + h_3 F_3(y_3, \varepsilon_3)), \end{aligned} \tag{3.27}$$

where $F_3(y_3, \varepsilon_3) = 1 - y_3^2 + \lambda\varepsilon_3$. For any h_3 system (3.27) has the fixed points

$$v_{r,3}^- = (0, -1, 0, h_3), \quad v_{r,3}^+ = (0, 1, 0, h_3).$$

The points $v_{r,3}^-$ and $v_{r,3}^+$ have a three-dimensional centre eigenspace and a one-dimensional unstable eigenspace with the eigenvalue $1 + 2h_3$. Hence, unlike the analogous case in the chart K_1 , the stability does not depend on the size of h_3 . The most relevant manifold for our problem is given by

$$W := \{w^{\text{out}}(h_3) := (0, 0, 0, h_3) \quad h_3 \in [0, \nu]\},$$

which is a line for system (3.27) within D_3 . The points $w^{\text{out}}(h_3)$ have two stable and two unstable eigenvalues

$$\lambda_1 = (1 + h_3)^{-2}, \quad \lambda_2 = (1 + h_3)^{-1}, \quad \lambda_3 = 1 + h_3, \quad \lambda_4 = 1 + 2h_3,$$

such that the stability corresponds to the time-continuous problem independently from h_3 . Note that the chart K_3 differs in that respect from the chart K_1 where preservation of stability is bound to the stability criteria of the Euler method known from the Dahlquist test equation.

The eigenvalues λ_1, λ_2 correspond with the ε_3 - and y_3 -directions and λ_3, λ_4 with the r_3 - and h_3 -directions. We extend the set W to the attracting invariant manifold $M_{a,3}$, which is given in D_3 by a graph $y_3 = l_3(\varepsilon_3, h_3)$. One can derive l_3 from the discrete invariance equation

$$l_3(\tilde{\varepsilon}_3, \tilde{h}_3) = \frac{l_3(\varepsilon_3, h_3) + \varepsilon_3 h_3}{1 + h_3 F_3(l_3(\varepsilon_3, h_3), \varepsilon_3)}. \tag{3.28}$$

Note that, analogously to the continuous time case, there is the resonance $\lambda_1 \lambda_3 = \lambda_2$, which makes the description of the dynamics close to W and $M_{a,3}$ a delicate problem. However, the exiting behaviour can still be estimated by a relatively simple argument without a full analysis of the resonance as follows. Let P_3 denote the map given by (3.27) and π_y the projection to the y -component.

Proposition 3.9. *The transition map Π_3 from Σ_3^{in} to the vicinity of Σ_3^{out} given by*

$$\Pi_3(z) = P^{m^*(z)}(z), \text{ where } m^*(z) = \arg \min_{n \in \mathbb{N}} \text{dist}(P_3^n(z), \Sigma_3^{\text{out}}), \text{ } z \in \Sigma_3^{\text{in}},$$

is well-defined on $k_{23}(\Sigma_{2,e}^{\text{out}})$. Furthermore, for $z \in k_{23}(\Sigma_{2,e}^{\text{out}}) \subset \Sigma_3^{\text{in}}$ we have $\pi_y(\Pi_3(z)) = \mathcal{O}(\delta^{1/3})$.

Proof. By the construction of $\Sigma_{2,e}^{\text{out}}$, Proposition 3.6, and the fact that $y_3 = x_2^{-1}y_2$ we have $\pi_y(z) = \mathcal{O}(\delta^{1/3})$ for any $z \in k_{23}(\Sigma_{2,e}^{\text{out}})$. Further note that F_3 is clearly positive as long as y_3 maintains some positive order of δ . Since $\varepsilon_3 h_3 = \mathcal{O}(\delta\nu)$ in D_3 , we can immediately infer that

$$\pi_y(P_3^n(z)) = \mathcal{O}(\delta^{1/3}) \quad \text{for all } n \leq m^*(z).$$

This implies both statements as F_3 stays positive along the trajectory. □

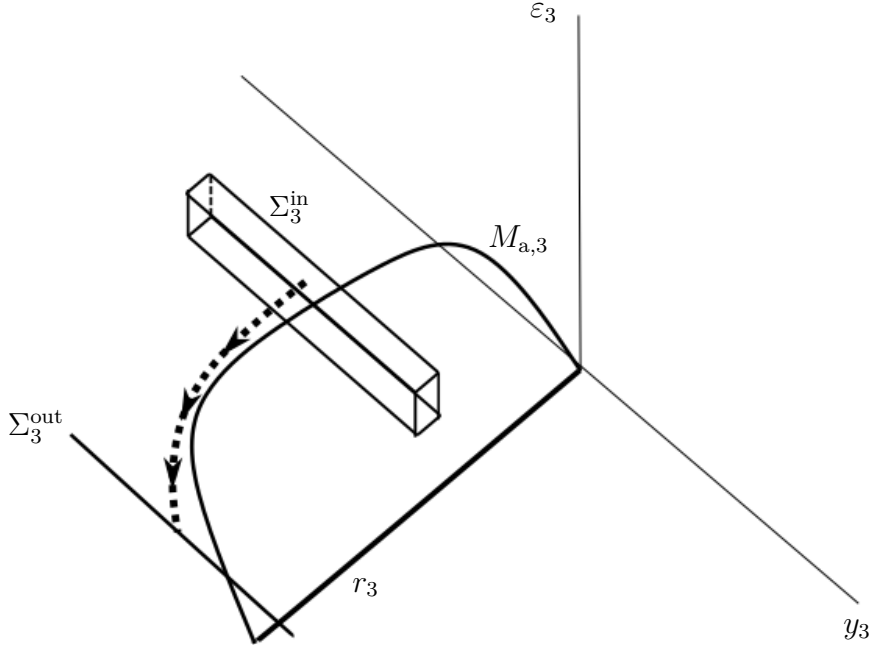


Figure 6: Illustration of the dynamics in chart K_3 in $(r_3, y_3, \varepsilon_3)$ -space. Note that, due to the relation $h_3 = r_3 h$, we can interpret $l_3(\varepsilon_3, h_3)$ as a function of (ε_3, r_3) and sketch its graph, the invariant manifold $M_{a,3}$, as in the figure above. The figure shows a trajectory (dotted line) starting in Σ_3^{in} up to reaching the vicinity of Σ_3^{out} close to $M_{a,3}$.

3.5 Connecting the charts and proof of the Theorem

Finally, we can prove Theorem 3.1 by combining the dynamics in K_1 , K_2 and K_3 into a global picture.

Proof of Theorem 3.1. We have proven the statements in charts K_1, K_2, K_3 for $\bar{\varepsilon} = \delta$ with δ sufficiently small. Hence, we choose $\varepsilon_0 = \rho^2 \delta_0$, where δ_0 is the largest value of $\delta/4$ such that the statements hold. We did not use any further restrictions on h apart from $\rho h < \delta$ and $\rho h < \frac{1}{8}$. Hence, it is enough to assume $\rho^3 h < \varepsilon$.

As before, we distinguish several cases. First, we consider $\lambda < 1$. We define the map $\bar{\Pi}_a$ from $R_1 \subset \Sigma_{1,-}^{\text{in}}$ to the vicinity of $\Sigma_{1,+}^{\text{out}}$ by

$$\bar{\Pi}_a := \Pi_{1,+} \circ k_{21} \circ \Pi_2 \circ k_{12} \circ \Pi_{1,-},$$

where $\Pi_2 : \Sigma_2^{\text{in}} \rightarrow \Sigma_{2,a}^{\text{out}}$ is the map well-defined by Proposition 3.6. We have seen that

$$k_{12}(\Pi_{1,-}(R_1)) \subset \Sigma_2^{\text{in}} \quad \text{and} \quad k_{21}(\Sigma_{2,a}^{\text{out}}) \subset R_2 \subset \Sigma_{1,+}^{\text{in}}.$$

Hence, $\bar{\Pi}_a$ is indeed a well-defined map. We have that $\Pi_a = \Phi \circ \bar{\Pi}_a \circ \Phi^{-1}$, where $\Delta^{\text{in}} = \Phi(R_1)$ and $\Delta_a^{\text{out}} \subset \Phi(\Sigma_{1,+}^{\text{out}})$ is an interval about S_a^+ of the same size as Δ^{in} . We observe with Proposition 3.2 that $\Phi(M_{a,1}^-) \subset S_{a,\varepsilon,h}^-$ and $\Phi(M_{a,1}^+) \subset S_{a,\varepsilon,h}^+$, and, by the choices of R_1 and R_2 , that $\Delta^{\text{in}} \cap S_{a,\varepsilon,h}^-$ and $\Pi_a(\Delta^{\text{in}}) \cap S_{a,\varepsilon,h}^+$ are nonempty. Summarizing, we can conclude that Π_a maps Δ^{in} including $\Delta^{\text{in}} \cap S_{a,\varepsilon,h}^-$ to a set about $S_{a,\varepsilon,h}^+$. The distance between any point in $\Pi_a(\Delta^{\text{in}})$ and Δ_a^{out} is of order $\mathcal{O}(h\varepsilon)$ since for $(x, y) \in \Delta_a^{\text{out}} \cap S_{a,\varepsilon,h}^+$ it is bounded by $h(x^2 - y^2 + \lambda\varepsilon)$ due to the definition of Π_a and we have by (3.15) that

$$|x^2 - y^2| = |x - y| |x + y| = \mathcal{O}(\delta\rho)\mathcal{O}(\rho) = \mathcal{O}\left(\frac{\varepsilon}{\rho}\right)\mathcal{O}(\rho) = \mathcal{O}(\varepsilon).$$

Furthermore, Proposition 3.5 says that $\Pi_{1,-}|R_1$ and $\Pi_{1,+}|R_2$ are contractions in the y_1 direction with rates of order at least $\mathcal{O}\left((1-c)^{\frac{C}{\rho h \delta}}\right)$ for some constant $C > 0$. Since Π_2 is also contracting and due to $\mathcal{O}(\delta) = \mathcal{O}\left(\frac{\varepsilon}{\rho^2}\right)$, we obtain that $\Pi_a(\Delta^{\text{in}})$ has y -width at most of order $\mathcal{O}\left((1-c)^{\frac{C\rho}{h\varepsilon}}\right)$.

Let now $\lambda > 1$. We define the map $\bar{\Pi}_e$ from $R_1 \subset \Sigma_{1,-}^{\text{in}}$ to the vicinity of Σ_3^{out} by

$$\bar{\Pi}_e := \Pi_3 \circ k_{23} \circ \Pi_2 \circ k_{12} \circ \Pi_{1,-}.$$

Again, we know that $k_{12}(\Pi_{1,-}(R_1)) \subset \Sigma_2^{\text{in}}$, and furthermore from Proposition 3.9 that Π_3 is well-defined on $k_{23}(\Sigma_{2,e}^{\text{out}}) \subset \Sigma_3^{\text{in}}$. Hence, $\bar{\Pi}_e$ is indeed a well-defined map. We have that $\Pi_e = \Phi \circ \bar{\Pi}_e \circ \Phi^{-1}$, where again $\Delta^{\text{in}} = \Phi(R_1)$ and $\Delta_e^{\text{out}} \subset \Phi(\Sigma_3^{\text{out}})$ is an interval perpendicular to the x -axis. It follows immediately that $S_{a,\varepsilon,h}^-$ passes through Δ_e^{out} at a point $(\rho, k(\varepsilon))$. Using Proposition 3.9 we can characterize $k(\varepsilon) = \rho\mathcal{O}(\delta^{1/3}) = \rho^{1/3}\mathcal{O}(\varepsilon^{1/3})$.

The fact that $\Pi_e(\Delta^{\text{in}})$ has y -width $\mathcal{O}\left((1-c)^{\frac{C\rho}{h\varepsilon}}\right)$ follows as for $\lambda < 1$. The distance between any point in $\Pi_e(\Delta^{\text{in}})$ and Δ_a^{out} is of order $\mathcal{O}(h(\varepsilon + \rho^2))$ since for $(x, y) \in \Delta_e^{\text{out}} \cap S_{a,\varepsilon,h}^-$ it is bounded by $h(x^2 - y^2 + \lambda\varepsilon)$ due to the definition of Π_e and $x^2 - y^2 = \mathcal{O}\left(\rho^2 - \varepsilon^{2/3}\rho^{2/3}\right)$. This finishes the proof. \square

4 Summary and Outlook

We have applied the blow-up method to the Euler discretization of a fast-slow system with a transcritical singularity at the origin. We have shown that the qualitative behaviour of the slow

manifolds is preserved by the discretization for any choice of $0 < h < \varepsilon$ (setting $\rho = 1$), where h denotes the time step size and ε the small time scaling parameter of the fast-slow system. The central part of the proof lies in the scaling chart K_2 of the manifold corresponding with the blown up singularity and is expressed in Proposition 3.6. The proof of the proposition uses direct analysis of the map and, by that, can be seen of an alternative way of also showing the continuous analogue of the result when $h \rightarrow 0$. Furthermore, we are able to estimate transition times of trajectories by the analysis of the entering chart K_1 and give a bound for the y -component in the exiting chart K_3 . In fact, our estimates provide a very fine control on individual trajectories, which is a potential advantage of the discrete-time framework for fast-slow systems.

We consider the work presented in this paper as one of the key steps towards a more comprehensive analysis of non-hyperbolic fixed points and non-hyperbolic submanifolds of fixed points in maps with multiple time scales. Whereas the normally hyperbolic theory for discrete-time multiple time scale systems is already quite well developed in [11, 25, 26], the geometric desingularisation of non-hyperbolic objects for maps still needs several extensions. For example, our problem (1.1) is based on an explicit Euler discretization, which is obviously the most straight forward scheme. We conjecture that one can use the more direct blow-up approach we use here for maps corresponding to ODEs also for other time-discretization schemes.

There are several reasons, why particular schemes should be checked: it is well-known from the area of geometric integration and the general theory of structure-preserving discretizations [10] that only certain discrete-time schemes preserve relevant dynamical properties, e.g. adiabatic invariants for the Hamiltonian systems case [10] or certain asymptotic dynamics for the dissipative case [12]. For multiple time scale maps, Runge-Kutta methods have been studied from a geometric viewpoint [23, 24]. It remains to clarify more systematically, for which discretization the geometric blow-up approach can be applied and what the relation between the two small parameters $0 < h, \varepsilon \ll 1$ must be. In this context, an interesting problem are canard explosions in discrete-time [6, 8], where also a third parameter is going to play a key role. Working out this case starting from the geometric approach by Krupa and Szmolyan for fast-slow ODEs [16] is currently work in progress by the authors of this paper.

References

- [1] E. Benoît, J.L. Callot, F. Diener, and M. Diener. Chasse au canards. *Collect. Math.*, 31:37–119, 1981.
- [2] G. G. Dahlquist. A special stability problem for linear multistep methods. *Nordisk Tidskr. Informations-Behandling*, 3:27–43, 1963.
- [3] F. Dumortier. *Singularities of vector fields*, volume 32 of *Monografías de Matemática [Mathematical Monographs]*. Instituto de Matemática Pura e Aplicada, Rio de Janeiro, 1978.
- [4] F. Dumortier. Techniques in the theory of local bifurcations: blow-up, normal forms, nilpotent bifurcations, singular perturbations. In *Bifurcations and periodic orbits of vector fields (Montreal, PQ, 1992)*, volume 408 of *NATO Adv. Sci. Inst. Ser. C Math. Phys. Sci.*, pages 19–73. Kluwer Acad. Publ., Dordrecht, 1993.
- [5] F. Dumortier and R. Roussarie. Canard cycles and center manifolds. *Mem. Amer. Math. Soc.*, 121(577):x+100, 1996. With an appendix by Cheng Zhi Li.
- [6] A. El-Rabih. Canards solutions of difference equations with small step size. *J. Difference Equ. Appl.*, 9(10):911–931, 2003.
- [7] N. Fenichel. Geometric singular perturbation theory for ordinary differential equations. *J. Differential Equations*, 31:53–98, 1979.
- [8] A. Fruchard. Canards discrets. *C. R. Acad. Sci. Paris Sér. I Math.*, 307(1):41–46, 1988.
- [9] I. Gucwa and P. Szmolyan. Geometric singular perturbation analysis of an autocatalator model. *Discr. Cont. Dyn. Syst. S*, 2(4):783–806, 2009.
- [10] E. Hairer, C. Lubich, and G. Wanner. *Geometric numerical integration*, volume 31 of *Springer Series in Computational Mathematics*. Springer, Heidelberg, 2010. Structure-preserving algorithms for ordinary differential equations, Reprint of the second (2006) edition.
- [11] M. W. Hirsch, C. C. Pugh, and M. Shub. *Invariant manifolds*. Lecture Notes in Mathematics, Vol. 583. Springer-Verlag, Berlin-New York, 1977.
- [12] S. Jin. Efficient asymptotic-preserving (AP) schemes for some multiscale kinetic equations. *SIAM J. Sci. Comput.*, 21(2):441–454, 1999.
- [13] C. K. R. T. Jones. Geometric singular perturbation theory. In *Dynamical systems (Montecatini Terme, 1994)*, volume 1609 of *Lecture Notes in Math.*, pages 44–118. Springer, Berlin, 1995.
- [14] M. Krupa and P. Szmolyan. Extending geometric singular perturbation theory to nonhyperbolic points—fold and canard points in two dimensions. *SIAM J. Math. Anal.*, 33(2):286–314, 2001.
- [15] M. Krupa and P. Szmolyan. Extending slow manifolds near transcritical and pitchfork singularities. *Nonlinearity*, 14(6):1473–1491, 2001.

- [16] M. Krupa and P. Szmolyan. Relaxation oscillation and canard explosion. *J. Differential Equations*, 174(2):312–368, 2001.
- [17] C. Kuehn. Normal hyperbolicity and unbounded critical manifolds. *Nonlinearity*, 27(6):1351–1366, 2014.
- [18] C. Kuehn. *Multiple time scale dynamics*, volume 191 of *Applied Mathematical Sciences*. Springer, Cham, 2015.
- [19] C. Kuehn. A remark on geometric desingularization of a non-hyperbolic point using hyperbolic space. *J. Phys. Conf. Ser.*, 727:012008, 2016.
- [20] P. De Maesschalck and F. Dumortier. Time analysis and entry-exit relation near planar turning points. *J. Difference Equ. Appl.*, 215:225–267, 2005.
- [21] P. De Maesschalck and F. Dumortier. Singular perturbations and vanishing passage through a turning point. *J. Differential Equations*, 248:2294–2328, 2010.
- [22] P. De Maesschalck and M. Wechselberger. Neural excitability and singular bifurcations. *J. Math. Neurosci.*, 5(1):16, 2015.
- [23] K. Nipp and D. Stoffer. Invariant manifolds and global error estimates of numerical integration schemes applied to stiff systems of singular perturbation type. I. RK-methods. *Numer. Math.*, 70(2):245–257, 1995.
- [24] K. Nipp and D. Stoffer. Invariant manifolds and global error estimates of numerical integration schemes applied to stiff systems of singular perturbation type. II. Linear multistep methods. *Numer. Math.*, 74(3):305–323, 1996.
- [25] K. Nipp and D. Stoffer. *Invariant manifolds in discrete and continuous dynamical systems*, volume 21 of *EMS Tracts in Mathematics*. European Mathematical Society (EMS), Zürich, 2013.
- [26] C. Pötzsche. Slow and fast variables in non-autonomous difference equations. *J. Difference Equ. Appl.*, 9(5):473–487, 2003. Dedicated to Professor George R. Sell on the occasion of his 65th birthday.
- [27] S. Wiggins. *Normally hyperbolic invariant manifolds in dynamical systems*, volume 105 of *Applied Mathematical Sciences*. Springer-Verlag, New York, 1994. With the assistance of György Haller and Igor Mezić.